

# Hydrothermal alteration of a chevkinite-group mineral to a bastnäsite-(Ce)-ilmenite- columbite-(Fe) assemblage: interaction with a F-, CO<sub>2</sub>-rich fluid

Ray Macdonald<sup>1,2</sup> · Bogusław Bagiński<sup>1</sup> · Pavel M. Kartashov<sup>3</sup> · Dmitry Zozulya<sup>4</sup> · Piotr Dzierżanowski<sup>1</sup> · Petras Jokubauskas<sup>1</sup>

Received: 18 December 2014 / Accepted: 24 June 2015 / Published online: 21 July 2015  
© The Author(s) 2015. This article is published with open access at Springerlink.com

**Abstract** The results are presented of a textural and mineral chemical study of a previously undescribed type of hydrothermal alteration of chevkinite-(Ce) which occurs in a syenitic pegmatite from the Vishnevye Mountains, Urals Region, Russia. The progressive alteration of the chevkinite to a bastnäsite-(Ce)-ilmenite-columbite-(Fe) assemblage through a series of texturally complex intermediate stages is described and electron microprobe analyses are given of all the major phases. Unusual Nb±Th-rich phases formed late in the alteration sequence provide evidence of local Nb mobility. The main compositional fluxes are traced, especially of the REE, HFSE, Th and U. It appears that almost all elements, with the exception of La, released from the chevkinite-(Ce) were reincorporated into later phases, such that they did not leave the alteration crust in significant amounts. The hydrothermal fluids are inferred to have been F- and CO<sub>2</sub>-rich, with variable levels of Ca activity, and with *f*O<sub>2</sub> mainly between the nickel-nickel oxide and magnetite-hematite buffers. This occurrence represents a new paragenesis for a columbite-group mineral.

Editorial handling: A. Beran

**Electronic supplementary material** The online version of this article (doi:10.1007/s00710-015-0394-2) contains supplementary material, which is available to authorized users.

✉ Ray Macdonald  
r.macdonald@lancaster.ac.uk

<sup>1</sup> Institute of Geochemistry, Mineralogy and Petrology, University of Warsaw, 02-089 Warsaw, Poland

<sup>2</sup> Environment Centre, Lancaster University, Lancaster LA1 4YQ, UK

<sup>3</sup> Institute of Ore Deposits, Russian Academy of Sciences, Moscow 109107, Russia

<sup>4</sup> Geological Institute, Kola Science Centre, Russian Academy of Sciences, Apatity, Russia

## Introduction

The two most abundant members of the chevkinite group of minerals (CGM) are chevkinite and perrierite, which have the general formula (REE,Ca)<sub>4</sub>Fe<sup>2+</sup>(Fe<sup>2+</sup>,Fe<sup>3+</sup>,Ti)<sub>2</sub>Ti<sub>2</sub>(Si<sub>2</sub>O<sub>7</sub>)<sub>2</sub>O<sub>8</sub>. It is important to understand the low-temperature alteration of the CGM for the following reasons. First, with ΣREE<sub>2</sub>O<sub>3</sub> contents up to 50 wt.%, members of the group have a high potential for REE mobilization during hydrothermal alteration and thus the mineralizing potential of the fluids. Second, the flexibility of the chevkinite lattice and its ability to incorporate a range of cations with variable charges and ionic radii may make it suitable for the incorporation of nuclear waste. Third, the CGM have the potential to be used for radiometric dating; Vazquez et al. (2014), for example, presented the results of ion microprobe <sup>238</sup>U-<sup>230</sup>Th dating of chevkinite from high-silica rhyolites of La Primavera caldera, Mexico, which were broadly consistent with corresponding K-Ar ages.

Several studies have addressed the hydrothermal alteration of chevkinite and perrierite. Kartashov (1994) reported on the alteration of chevkinite in metasomatic rocks of the Tsahirin-Khuduk ore occurrence, Khaldzan Buragtag massif, Mongolia. He considered that the alteration could be described by three reactions, dependent, *inter alia*, on the Ca/Na ratio of the metasomatised host rock and the H<sub>2</sub>O/CO<sub>2</sub> ratio of the incoming fluids. Jiang (2006) described the alteration of chevkinite-(Ce) to a corona of allanite-ilmenite-titanite-epidote-quartz by residual magmatic fluids and a later hydrothermal fluid in syenites of the Shuiquangou complex, China. In a study of A-type granites and syenites of the Graciosa Province, southern Brazil, Vlach and Gualda (2007) documented increases in Ti and reductions in REE and Fe resulting from interaction between chevkinite-(Ce) and post-magmatic hydrous fluids. Bagiński et al. (2015) and Macdonald et al. (2015) documented the alteration of

chevkinite-(Ce) to a phase strongly enriched in Ti (and to a lesser degree in Nb and Th) and depleted in Si, REE and Fe compared to the unaltered phase.

We now complement these studies by documenting a previously unrecorded type of interaction between a CGM and hydrothermal fluids, where chevkinite-(Ce) was altered to a bastnäsite-(Ce)-ilmenite-columbite-(Fe) assemblage *via* a complex series of intermediate steps which were arrested before equilibrium was achieved. In contrast to most previous studies of CGM alteration, the chevkinite-(Ce) did not alter to a member of the epidote-group, possibly because of a high  $\text{CO}_2/\text{H}_2\text{O}$  ratio in the hydrothermal fluids, as discussed below.

### Sample details

The material used in this study is from the Vishnevye (Cherry) Mountains, Chelyabinsk Oblast', southern Urals, Urals Region, Russia. The specimen (K4) comes from the collections of Pavel Kartashov. According to the label, it was collected in 1959 by P. Kalinin from vein #35. However, vein #35 is a very large nepheline-syenite pegmatite cutting across Dolgaya Mountain. Furthermore, the vein was exploited only from the mid-1960s. Alternatively, the specimen was collected from a small trench or surface exposure, or from a small pegmatite vein accompanying pegmatite #35 at its northern end. At present, this part of Dolgaya has been completely mined out by the quarry company and is buried under dumps.

Pegmatite #35 is a strongly carbonatized vein of miaskitic pegmatite, the carbonatization being relatively early in the alteration sequence (Es'kova et al. 1964). Nepheline and then microcline were replaced by calcite, with the formation of an apatite-biotite-calcite rock with some relict albite. The replacement was accompanied by the loss of Si, Al, K, Na and the addition of Ca, Sr, LREE, P and  $\text{CO}_2$ . Early carbonatization replaced significant volumes of felsic material, whereas a later phase of carbonatization resulted in the formation of small carbonate (calcite, ferrodolomite) and quartz veinlets.

Early carbonatization involved moderate concentrations of F in the fluid. Fluorite is a very minor phase in the albite-biotite-calcite rocks, the main concentrator of F being Sr- and LREE-bearing fluorapatite. Its abundance in such rocks reaches 15–20 vol.%. Biotite-apatite veins also are known as result of earlier carbonatization. Another concentrator of F is Ti-bearing annite. Fluorite is present here as a minor accessory phase but in the small veinlets of later carbonatization it is an abundant minor rock-forming phase. Overall, it appears that the fluids were alkaline, rich in Ca and  $\text{CO}_2$  and moderately rich in F.

Our specimen is from an aegirine-microcline syenite pegmatite containing a  $74 \times 2.5$  cm section of a large, single crystal of chevkinite-(Ce) (Fig. 1a). Along its boundary with the microcline matrix, the crystal has been replaced by a 5–12 mm

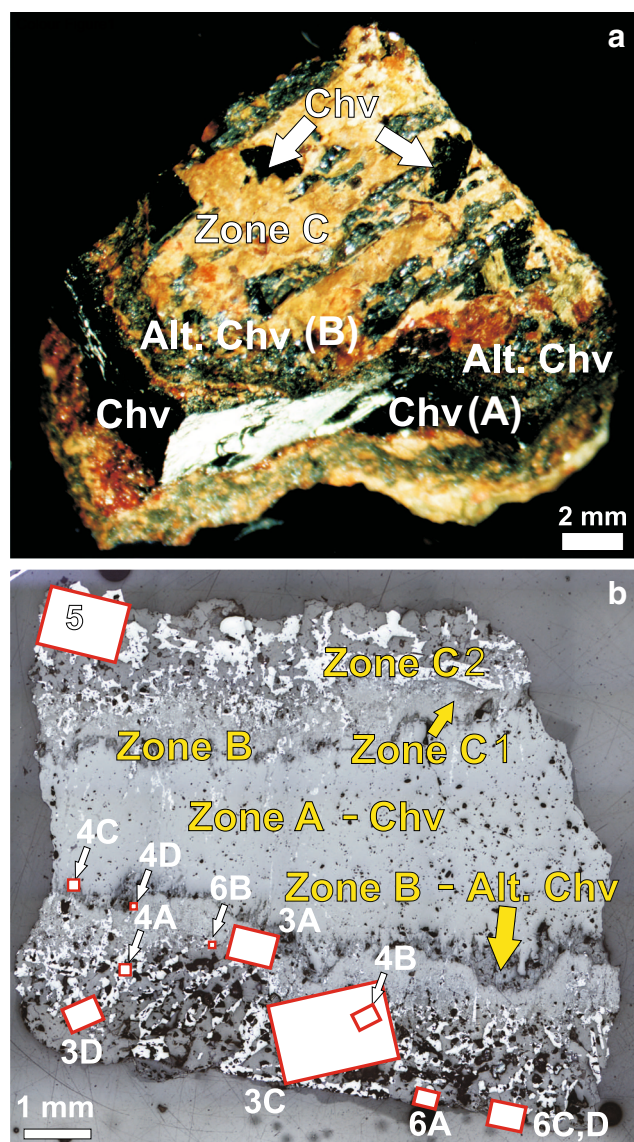


**Fig. 1** **a** Photograph of sample K4, showing the black, vitreous core of chevkinite-(Ce) (Chv; Zone A), the dark grey, mottled zone of altered chevkinite (Alt. Chv) (Zone B) and the bastnäsite-(Ce) + ilmenite alteration rim (Zones C1, C2). **b** Reflected light photomicrograph of thin section of K4, showing the relationships between the alteration zones. The bright veinlets in the top-left part of Zone A are bastnäsite-(Ce). The locations of Figs. 3, 4, 5 and 6 are marked

zone of ilmenite-bastnäsite-(Ce) composition. Up to 25–30 vol.% of the original chevkinite crystal was replaced. Given their close association, we may infer that the replacement of the chevkinite was contemporary with the carbonatization of pegmatite #35 and under the influence of the same fluids.

### Analytical methods

Mineral compositions were determined by electron microprobe at the Inter-Institute Analytical Complex at the Faculty

of Geology, University of Warsaw, using a Cameca SX-100 microprobe equipped with three wavelength dispersive spectrometers. The conditions used for analysis of chevkinite were: accelerating voltage 15 kV and the probe current 20 or 40 nA. Counting times were 20 s on peak and 10 s on each of two background positions. The standards, crystals and X-ray lines used and detection limits are given in the Appendix. The 'PAP' $\phi(\rho Z)$  program (Pouchou and Pichoir 1991) was used for corrections. The analytical conditions differed for the other phases: details may be obtained from the authors. Representative analyses of all phases are presented in Tables 1, 2, 3, 4, 5, 6, 7 and 8; the full data set is given in Supplementary Tables 1–3.

Quantitative element distribution maps were acquired in the Cryo-SEM laboratory, Faculty of Geology, University of Warsaw, using a Zeiss Sigma<sup>TM</sup> VP FE (field emission) – SEM equipped with new generation SDD-type two EDS (XFlash 6|10<sup>TM</sup>) detectors produced by Bruker. An acceleration voltage of 30 kV and a 120  $\mu\text{m}$  aperture with high current option ensured the effective generation of X-rays from heavy elements (Ce and Th). EDS electron throughput and X-ray signal amplification were configured to keep dead time below 8 %. 8 $\times$ 9 tiles (256 $\times$ 196 pixel/12.5 min. per tile) were mapped using automatic Bruker Esprit<sup>®</sup> software functionality, but final element distribution mosaics were assembled using a custom-written Python<sup>TM</sup> script, and visualised by Gwyddion software (Nečas and Klapetek 2012).

A note on mineral nomenclature is required. Without XRD confirmation of the structure, it is not known whether the ThSiO<sub>4</sub> phase in K4 is thorite (tetragonal) or its dimorph huttonite (monoclinic). The phase is here simply termed ThSiO<sub>4</sub>.

## Textural details

The varying mineral assemblages are described as a series of zones (A, B, C1 and C2), which were formed sequentially during the progressive fluid-induced alteration of an initial magmatic chevkinite-(Ce) crystal. Unusually, perhaps uniquely, an opportunity has been provided by this crystal to see all stages of a previously unrecorded alteration process in this phase.

Sample K4 has a core of lustrous black to cherry-red chevkinite-(Ce) surrounded by an alteration crust dominantly of yellow bastnäsite-(Ce) and ilmenite (Fig. 1a). Figure 1b shows the thin alteration rim surrounding the chevkinite-(Ce). The unaltered chevkinite-(Ce) (Zone A) is bordered, and penetrated, by a thin, heterogeneous, sinuous, partly stringy zone (B), dark-grey on back-scattered electron (BSE) images, of altered chevkinite (Fig. 2). Zone C1 comprises a very fine-grained layer which becomes coarser into Zone C2. Zone C1 is very difficult to resolve in our BSE

images but from its bulk composition (see below), it is taken to be a REE-carbonate. The transition from unaltered chevkinite-(Ce) to the alteration rim is shown in more detail in Fig. 2a. The altered phase penetrates into the unaltered phase as thin veinlets and is itself cut by veins of bastnäsite-(Ce), ilmenite and ThSiO<sub>4</sub> (Fig. 2b). In further detail (Fig. 2c), the heterogeneity of the altered chevkinite (Zone B) is marked by rapid variations in BSE intensity; it also includes small residual patches of chevkinite-(Ce). Note the general, but variable, coarsening of Zone C1 into Zone C2, marked by a sharp increase in grain size, and the veins of carbonate penetrating C1. Stringers containing ThSiO<sub>4</sub> cut the boundary between Zones A and B and also occur in some carbonate veins (Figs. 2b and c). Patches with a symplectite texture have developed locally in the transition between Zones C1 and C2 (Fig. 3a and b). They are up to ~200  $\mu\text{m}$  across and usually rather rounded; the example shown in Fig. 3 is fan-shaped and measures 160 $\times$ 100  $\mu\text{m}$ . They consist mainly of finely intergrown ilmenite and bastnäsite-(Ce). We speculate that the texture was formed by local rapid loss of volatiles.

The main part of the alteration crust (Zone C2) is composed of an interlocking mosaic of ilmenite, bastnäsite-(Ce), columbite-(Fe) and quartz, with scattered crystals of aegirine and ThSiO<sub>4</sub> (Fig. 3c). The ilmenite has a homogeneous grey appearance on BSE images; the REE-carbonate is generally bright but commonly shows complex zoning, with twinned dark areas intergrown with lighter, slightly patchy areas (Fig. 3d). The columbite-(Fe) forms small (<40  $\mu\text{m}$ ), rounded grains normally enclosed in either ilmenite or bastnäsite-(Ce) or grown along the contact between them. It is almost invariably zoned, as revealed by differences in BSE intensity. The nature of the zoning in the columbite-(Fe) is variable. In the upper right part of the crystal shown in Fig. 4a, a dark core is mantled by a patchily zoned, rather brighter zone. A bright vein cuts the core. The lower left part has patches of bright and dark phases, mantled by a more homogeneous material. The crystal shown in Fig. 4b comprises an oscillatory zoned region overprinted by a darker (lower Z) phase. The presence of veinlets indicates that the brighter material generally replaced the darker. As far as we know, this occurrence of columbite represents a new paragenesis for the mineral.

Aegirine mainly forms crystals located between ilmenite and carbonate crystals (Fig. 3c). With the exception of a few crystals, it is altered to a material which superficially looks homogeneous but is actually composed of an interlocking mesh of acicular phases, up to 5  $\mu\text{m}$  long, that we have not yet resolved but may be phyllosilicates. Quartz crystals are found throughout Zone C2, often growing along the contacts between the REE-carbonate and ilmenite (Fig. 2a).

ThSiO<sub>4</sub> occurs in several forms, including sub-prismatic to rounded grains in chevkinite-(Ce) (Fig. 4c), strings of small crystals in the altered chevkinite zone (Fig. 2b and c), and crystals associated with REE-carbonates and ilmenite in

**Table 1** Representative compositions of chevkinite-(Ce) and altered chevkinite in K4

	Profile through unaltered chevkinite				Random points in altered chevkinite			
	1	2	3	4	5	6	7	8
wt. %								
P <sub>2</sub> O <sub>5</sub>	bd	bd	bd	0.23	0.13	0.13	0.14	0.14
Nb <sub>2</sub> O <sub>5</sub>	2.09	2.01	2.21	3.06	5.23	5.09	4.39	5.27
Ta <sub>2</sub> O <sub>5</sub>	0.09	0.08	0.11	0.05	0.08	0.08	0.100	0.11
SiO <sub>2</sub>	18.78	18.86	18.82	15.79	17.98	18.63	14.64	19.94
TiO <sub>2</sub>	15.56	15.51	15.41	26.35	38.51	35.94	32.96	34.05
ZrO <sub>2</sub>	0.24	0.21	0.35	0.37	0.73	0.58	0.53	0.60
ThO <sub>2</sub>	2.94	2.93	2.74	3.38	8.11	7.79	6.48	7.21
UO <sub>2</sub>	bd	bd	bd	bd	bd	bd	bd	bd
Al <sub>2</sub> O <sub>3</sub>	0.19	0.22	0.20	1.34	0.34	0.40	0.32	0.45
Y <sub>2</sub> O <sub>3</sub>	bd	bd	bd	bd	bd	bd	bd	bd
La <sub>2</sub> O <sub>3</sub>	16.09	16.22	15.84	2.39	1.35	1.32	2.17	1.66
Ce <sub>2</sub> O <sub>3</sub>	20.17	20.49	20.36	12.42	6.67	5.64	9.64	7.33
Pr <sub>2</sub> O <sub>3</sub>	1.32	1.17	1.52	bd	bd	bd	0.19	bd
Nd <sub>2</sub> O <sub>3</sub>	2.94	2.83	2.54	0.62	0.57	0.48	0.60	0.72
Sm <sub>2</sub> O <sub>3</sub>	0.22	bd	bd	bd	0.20	0.16	bd	bd
Gd <sub>2</sub> O <sub>3</sub>	0.16	bd	bd	bd	bd	bd	bd	0.19
MgO	0.20	0.20	0.19	3.51	0.03	0.05	0.05	0.08
CaO	2.79	2.83	2.76	2.21	2.61	2.41	2.40	2.28
MnO	0.87	0.90	0.89	0.09	bd	bd	bd	bd
FeO*	11.22	11.14	11.42	7.31	5.13	4.76	5.48	5.39
SrO	0.44	0.46	0.49	0.07	0.12	0.13	0.15	0.23
BaO	0.13	0.14	0.21	0.94	1.61	1.53	1.27	1.26
Total	96.44	96.20	96.06	80.13	89.40	85.12	81.51	86.91
Formulae based on 22 oxygens								
Ca	0.648	0.658	0.642	0.509	0.522	0.499	0.549	0.466
Ba	0.011	0.012	0.018	0.079	0.118	0.116	0.106	0.094
La	1.287	1.298	1.268	0.190	0.093	0.094	0.171	0.117
Ce	1.601	1.628	1.618	0.978	0.456	0.399	0.753	0.512
Pr	0.104	0.092	0.120	0.000	0.000	0.000	0.015	0.000
Nd	0.228	0.219	0.197	0.048	0.038	0.033	0.046	0.049
Sm	0.016	0.000	0.000	0.000	0.013	0.011	0.000	0.000
Gd	0.011	0.000	0.000	0.000	0.000	0.000	0.000	0.012
Y	0.000	0.000	0.000	0.000	0.000	0.000	0.000	0.000
Th	0.145	0.145	0.135	0.165	0.344	0.343	0.315	0.313
U	0.000	0.000	0.000	0.000	0.000	0.000	0.000	0.000
Sum A	4.052	4.052	3.998	1.969	1.584	1.495	1.955	1.563
Fe <sup>2+</sup>	1.000	1.000	1.000	1.000	0.801	0.770	0.978	0.860
Mn	0.000	0.000	0.000	0.000	0.000	0.000	0.000	0.000
Mg	0.000	0.000	0.000	0.000	0.008	0.014	0.016	0.023
Sum B	1.000	1.000	1.000	1.000	0.809	0.784	0.994	0.883
Fe <sup>2+</sup>	1.034	1.021	1.072	0.314	0.000	0.000	0.000	0.000
Mn	0.160	0.165	0.164	0.016	0.000	0.000	0.000	0.000
Mg	0.065	0.065	0.061	1.125	0.000	0.000	0.000	0.000
Zr	0.025	0.022	0.037	0.039	0.066	0.055	0.055	0.056
Nb	0.205	0.197	0.217	0.297	0.441	0.445	0.424	0.455
Ta	0.005	0.005	0.006	0.003	0.004	0.004	0.006	0.006

**Table 1** (continued)

	Profile through unaltered chevkinite				Random points in altered chevkinite			
	1	2	3	4	5	6	7	8
Al	0.049	0.056	0.051	0.340	0.075	0.091	0.081	0.101
Ti	0.537	0.530	0.515	2.261	3.405	3.225	3.291	2.885
Sum C	2.079	2.061	2.124	4.395	3.992	3.820	3.856	3.502
Ti (=D)	2.000	2.000	2.000	2.000	2.000	2.000	2.000	2.000
Si	4.071	4.091	4.084	3.395	3.355	3.601	3.125	3.804
P	0.000	0.000	0.000	0.058	0.029	0.030	0.035	0.031
Sum T	4.071	4.091	4.084	3.453	3.384	3.631	3.160	3.835
Σ cations	13.20	13.20	13.21	12.82	11.77	11.73	11.97	11.78

*FeO\** all Fe as  $Fe^{2+}$ , *bd* below detection

**Table 2** Representative analyses of REE-carbonates in K4

	1	2	3	4	5	6	7	8
wt. %								
SiO <sub>2</sub>	0.15	0.19	bd	bd	bd	0.22	0.50	0.28
ThO <sub>2</sub>	2.95	1.57	0.71	0.68	bd	16.32	27.97	7.50
Y <sub>2</sub> O <sub>3</sub>	bd	0.21	bd	bd	bd	0.29	0.24	0.40
La <sub>2</sub> O <sub>3</sub>	31.56	30.44	30.64	28.69	22.08	18.83	15.32	21.63
Ce <sub>2</sub> O <sub>3</sub>	38.41	40.26	35.52	35.89	32.56	25.53	19.82	29.50
Pr <sub>2</sub> O <sub>3</sub>	2.08	2.09	2.36	2.06	1.97	1.47	bd	1.18
Nd <sub>2</sub> O <sub>3</sub>	4.40	6.42	3.83	5.21	5.08	2.42	1.75	4.17
Sm <sub>2</sub> O <sub>3</sub>	0.55	bd	0.57	bd	bd	bd	bd	bd
CaO	0.98	0.30	bd	bd	6.83	4.75	5.76	4.74
FeO*	bd	0.36	bd	bd	bd	bd	0.93	0.22
SrO	bd	bd	bd	bd	0.73	0.75	1.31	0.68
F	10.17	10.60	9.34	8.76	5.78	6.53	5.20	6.97
Sum	91.25	92.44	82.97	81.29	75.03	77.11	78.80	77.27
O = F	4.28	4.46	3.93	3.69	2.43	2.75	2.19	2.93
Total	86.97	87.98	79.04	77.60	72.60	74.36	76.61	74.34
Formulae on basis of 1 cation								
Si	0.005	0.006	0.000	0.000	0.000	0.008	0.018	0.010
Th	0.022	0.012	0.006	0.006	0.000	0.136	0.225	0.060
Y	0.000	0.004	0.000	0.000	0.000	0.006	0.005	0.007
La	0.387	0.370	0.420	0.400	0.268	0.254	0.200	0.279
Ce	0.467	0.486	0.484	0.496	0.393	0.342	0.257	0.378
Pr	0.025	0.025	0.032	0.028	0.024	0.020	0.000	0.015
Nd	0.052	0.076	0.051	0.070	0.060	0.032	0.022	0.052
Sm	0.006	0.000	0.007	0.000	0.000	0.000	0.000	0.000
Ca	0.035	0.011	0.000	0.000	0.241	0.186	0.219	0.178
Fe <sup>2+</sup>	0.000	0.010	0.000	0.000	0.000	0.000	0.028	0.006
Sr	0.000	0.000	0.000	0.000	0.014	0.016	0.027	0.014
F	1.069	1.106	1.098	1.046	0.602	0.756	0.582	0.772
OH	0.000	0.000	0.000	0.000	0.398	0.244	0.418	0.228

Explanation: 1, 2, 3, 4 - anhedral plates in Zone C2; 5, darker phase replacing bastnäsinite-(Ce); 6, 7, lighter veinlets in Th-rich phase (Fig. 5b); 8, anhedral grain in texturally complex part of Zone C1 *FeO\**, all Fe as  $Fe^{2+}$ , *bd* below detection. OH contents calculated from the difference to unity at the OH-F site. Fluorine values exceeding unity may be a result of the overlap of F with the analytical peak of Ce

**Table 3** Representative compositions of ilmenite in K4

	Zone C2				Zones C1/C2 transition		associated with carbonate veins, Zone B			
	1	2	3	4	5	6	7	8	9	10
Nb <sub>2</sub> O <sub>5</sub>	0.64	0.55	0.82	1.23	6.81	8.06	1.34	3.72	0.68	1.04
SiO <sub>2</sub>	bd	bd	bd	bd	bd	0.10	bd	0.22	0.18	0.08
TiO <sub>2</sub>	51.35	51.86	51.69	51.04	49.05	46.40	51.47	48.82	52.71	51.17
MgO	0.04	0.04	0.03	0.02	bd	bd	0.02	bd	0.01	bd
CaO	bd	bd	bd	bd	bd	0.03	0.02	0.15	0.04	0.04
MnO	1.81	1.77	1.93	1.91	9.22	22.42	3.83	16.82	4.56	3.57
FeO*	45.11	44.55	44.04	44.06	31.34	18.21	39.42	23.42	37.63	38.43
Total	98.95	98.77	98.51	98.26	96.42	95.22	96.10	93.15	95.81	94.33
Formulae on basis of 3 oxygens										
Si	0.000	0.000	0.000	0.000	0.000	0.003	0.000	0.006	0.005	0.002
Ti	0.987	0.999	0.995	0.990	0.992	0.951	1.023	1.008	1.049	1.036
Fe <sup>3+</sup>	0.018	0.000	0.000	0.000	0.000	0.000	0.000	0.000	0.000	0.000
Fe <sup>2+</sup>	0.946	0.959	0.942	0.949	0.782	0.436	0.936	0.619	0.950	0.956
Mn	0.039	0.038	0.042	0.042	0.210	0.517	0.086	0.391	0.102	0.081
Mg	0.002	0.002	0.001	0.001	0.000	0.000	0.001	0.000	0.000	0.000
Ca	0.000	0.000	0.010	0.000	0.000	0.001	0.001	0.004	0.001	0.001
Nb	0.008	0.007	0.011	0.016	0.094	0.113	0.018	0.053	0.009	0.014
Σ cations	2.00	2.01	2.00	2.00	2.08	2.02	2.07	2.08	2.12	2.09
X <sub>ilm</sub>	99	100	101	100	105	102	104	107	106	105

FeO\* all Fe as Fe<sup>2+</sup>, bd below detection. Further details may be found in Supplementary Table 1c

Zone C2. Crystals tend to be partly resorbed, patchily zoned, and porous. As examples, the fractured, sub-prismatic crystal in Fig. 4c consists of a lighter grey, relatively homogeneous component largely replaced by a darker porous material, whilst the crystal in Fig. 4d, again patchily zoned, contains abundant pores and micropores. One crystal of monazite has been identified in Zone C2; it is partly resorbed and shows traces of oscillatory zoning. It has sharp contacts with ilmenite and bastnäsite-(Ce) and was presumably coeval with them. An analysis is provided in Supplementary Table 2c.

Throughout Zone C2, but concentrated towards the rim, the REE-carbonate is partially replaced by a lower-Z carbonate phase (Fig. 5a). The carbonate crystal shown in Fig. 5b has been veined and patchily replaced by a higher-Z, Th-rich phase which also forms the lining to the vug-like holes. Niobian rutile forms anhedral grains up to 20 µm across in coarser zones in the complex area immediately above Zone C1. It persists, but with finer grain size, to the boundary with the main alteration crust.

Niobium-rich oxide phases occur in three forms. First, a large (300×250 µm) quartz crystal at the rim of the alteration crust (Zone C2) has been patchily replaced by loosely connected patches of a phase taken to be a member of the pyrochlore supergroup (Pcl? Fig. 6a). The phase is heterogeneous, three areas with different intensities

being distinguishable. The first forms homogeneous grey areas; the second has slightly lower intensities. The third type has the highest Z and forms veins and patches cutting the other types. A typical example of the second type of Nb-rich material forms a wedge interstitial to bastnäsite-(Ce) crystals (Fig. 6b) in Zone C2, although broadly similar material also occurs associated with symplectites at the C1/C2 transition (Fig. 3b). The two main textural types are a blocky, homogeneous, grey phase and a grey phase with thin bright rims which penetrates the first as fingers and patches. The nature of this material is enigmatic. There are certain textural similarities between the mosaics and the aggregated spheres of ThSiO<sub>4</sub> found by Seydoux-Guillaume et al. (2007) in monazite from Arendal, Norway, which they suggested were very similar to a gel. The intriguing possibility is raised, therefore, that these, and perhaps other, phases in the texturally complex part of Zones C1 and C2, were never crystalline but formed from amorphous gels. Third, a Nb-rich phase locally forms a thin (~20 µm) layer replacing quartz at the outer rim of the alteration crust (Fig. 6c). At one end, the layer breaks down into a series of veinlets cutting a zircon crystal, the only zircon crystal found in the sample. Veinlets also cut an ilmenite crystal (lower left). Altered aegirine occurs at the tips of

**Table 4** Representative analyses of columbite-(Fe) in K4

	1	2	3	4	5	6	7	8
wt. %								
WO <sub>3</sub>	0.48	0.83	0.94	0.83	0.88	0.93	1.07	1.09
P <sub>2</sub> O <sub>5</sub>	bd	0.05	0.04					
Nb <sub>2</sub> O <sub>5</sub>	71.09	72.52	75.48	73.66	74.38	74.32	75.94	72.22
Ta <sub>2</sub> O <sub>5</sub>	0.27	0.56	0.28	0.47	0.42	0.45	0.24	0.48
SiO <sub>2</sub>	0.02	0.02	bd	bd	bd	bd	bd	bd
TiO <sub>2</sub>	3.94	2.99	1.95	3.20	2.86	3.06	2.05	3.71
ZrO <sub>2</sub>				0.19	0.10	0.16	0.04	0.16
ThO <sub>2</sub>	1.13	0.96	0.39	0.95	1.57	1.30	bd	0.88
Al <sub>2</sub> O <sub>3</sub>	bd	bd	0.04					
Sc <sub>2</sub> O <sub>3</sub>	0.53	0.40	0.41	0.45	0.25	0.14	0.16	0.19
Y <sub>2</sub> O <sub>3</sub>	1.41	0.77	0.27	1.02	0.59	0.59	0.12	0.95
La <sub>2</sub> O <sub>3</sub>	bd	bd	bd	0.11	bd	0.07	bd	bd
Ce <sub>2</sub> O <sub>3</sub>	0.11	0.18	0.08	0.21	0.25	0.12	bd	0.22
Nd <sub>2</sub> O <sub>3</sub>	0.59	0.21	0.40	0.54	0.36	0.36	bd	0.72
Sm <sub>2</sub> O <sub>3</sub>	bd	bd	bd	0.30	0.19	0.26	bd	0.43
Gd <sub>2</sub> O <sub>3</sub>	0.46	0.23	0.15	0.27	0.27	0.17	bd	0.37
Dy <sub>2</sub> O <sub>3</sub>	0.40	0.48	bd					
Yb <sub>2</sub> O <sub>3</sub>	0.35	0.28	bd					
MgO	0.04	0.06	0.05	0.03	0.03	0.03	0.05	0.04
CaO	0.67	0.36	0.14	0.34	0.36	0.38	bd	0.48
MnO	8.17	9.58	9.90	9.98	9.23	9.55	10.03	8.82
FeO*	8.53	8.45	9.66	8.54	9.16	9.00	10.45	9.19
Total	98.19	98.93	100.18	100.90	100.90	100.89	100.15	99.95
Formulae on basis of 6 oxygens								
Ca	0.041	0.022	0.008	0.020	0.022	0.023	0.000	0.029
La	0.000	0.000	0.000	0.000	0.000	0.000	0.000	0.000
Ce	0.002	0.004	0.002	0.004	0.005	0.002	0.000	0.005
Nd	0.012	0.004	0.008	0.011	0.007	0.007	0.000	0.015
Gd	0.009	0.004	0.003	0.005	0.005	0.003	0.000	0.007
Dy	0.007	0.009	0.000					
Yb	0.006	0.005	0.000					
Y	0.043	0.023	0.008	0.030	0.018	0.018	0.004	0.029
Th	0.015	0.012	0.005	0.012	0.020	0.017	0.000	0.011
Fe <sup>2+</sup>	0.408	0.403	0.453	0.400	0.430	0.422	0.489	0.436
Mn	0.396	0.462	0.470	0.473	0.439	0.454	0.476	0.423
Sc	0.026	0.020	0.020	0.022	0.012	0.007	0.008	0.009
Mg	0.003	0.005	0.004	0.003	0.003	0.003	0.004	0.003
Al	0.000	0.000	0.003					
W	0.004	0.007	0.008	0.007	0.007	0.008	0.009	0.009
Ti	0.170	0.128	0.082	0.135	0.121	0.129	0.086	0.158
Nb	1.840	1.869	1.915	1.865	1.887	1.885	1.922	1.851
Ta	0.004	0.009	0.004	0.007	0.006	0.007	0.004	0.007
Zr				0.000	0.003	0.004	0.001	0.004
Si	0.001	0.001	0.000	0.000	0.000	0.000	0.000	0.000
P	0.000	0.002	0.002					
Σ cations	2.99	2.99	2.99	2.99	2.98	2.99	3.00	3.00

*FeO\** all Fe as Fe<sup>2+</sup>, *bd* below detection. Blank, not determined. Descriptions: analyses 1, 2, 3, small rounded blebs associated with ilmenite; 4, fractured anhedral crystal; 5, 6, patchily zoned, anhedral prism; 7, anhedral grain in patchy zone; 8, strongly zoned crystal

**Table 5** Compositions of aegirine and altered aegirine in K4

	Aegirine		Altered aegirine					
	1	2	3	4	5	6	7	8
wt. %								
Nb <sub>2</sub> O <sub>5</sub>							0.65	0.65
Ta <sub>2</sub> O <sub>5</sub>							0.19	0.29
SiO <sub>2</sub>	51.90	51.91	48.91	49.43	52.09	49.89	44.22	46.00
TiO <sub>2</sub>	0.30	0.30	0.75	0.66	0.41	0.09	0.30	0.60
Al <sub>2</sub> O <sub>3</sub>	0.37	0.37	5.52	5.83	6.15	5.73	5.21	6.26
Cr <sub>2</sub> O <sub>3</sub>	0.32	0.26						
Fe <sub>2</sub> O <sub>3</sub> *	30.41	31.02	32.41	32.60	33.32	30.29	31.35	30.82
MgO	0.49	0.53	0.74	0.83	0.34	0.20	0.62	0.38
CaO	1.44	1.51	0.84	0.66	0.51	0.26	1.01	0.63
MnO	0.13	0.16	0.11	bd	bd	bd	0.05	0.06
Na <sub>2</sub> O	12.57	12.46	0.06	bd	bd	bd	bd	bd
K <sub>2</sub> O	bd	bd	0.45	0.44	0.07	0.04	bd	bd
Total	97.93	98.52	89.79	90.45	92.89	86.50	83.60	85.69
Formulae on basis of 6 oxygens								
Si	2.020	2.011	1.986	1.988	2.025	2.067	1.945	1.958
Ti	0.009	0.009	0.023	0.020	0.012	0.003	0.010	0.019
Nb							0.013	0.013
Ta							0.002	0.003
Al	0.017	0.017	0.264	0.276	0.282	0.280	0.270	0.314
Cr	0.010	0.008						
Fe <sup>3+</sup>	0.891	0.904	0.991	0.987	0.974	0.944	1.038	0.987
Mn	0.004	0.005	0.004	0.000	0.000	0.000	0.002	0.002
Mg	0.028	0.031	0.045	0.050	0.020	0.012	0.041	0.024
Ca	0.060	0.063	0.037	0.028	0.021	0.012	0.048	0.029
Na	0.948	0.936	0.005	0.000	0.000	0.000	0.000	0.000
K	0.000	0.000	0.023	0.023	0.003	0.002	0.000	0.000
Σ cations	3.99	3.98	3.38	3.37	3.34	3.32	3.37	3.35

Descriptions: analyses 1, 2, ragged grain, intergrown with quartz (133×67 μm); 3, 4, crystal associated with ilmenite (240×200 μm); 5, 6, rectangular crystal with ilmenite and carbonate (215×143 μm); 7, in symplectite; 8, in wedge between ilmenite and carbonate. Fe<sub>2</sub>O<sub>3</sub>\* all Fe as Fe<sup>3+</sup>, bd below detection

two residual quartz layers. In more detail (Fig. 6d), the zircon and columbite-(Fe) are in contact with an unidentified Th-rich material (marked ?) comprising a patchy intergrowth of components with different Z. The bright grains are ThSiO<sub>4</sub>, presumably formed during alteration of the host.

## Mineral compositions

### Chevkinite-(Ce) and altered chevkinite

Eight new determinations of chevkinite-(Ce) from Zone A, determined along the profile shown in Fig. 2b, are presented in Table 1, and supplemented in Supplementary Table 1a by five analyses from Macdonald et al. (2012). The phase has been

classified as chevkinite-(Ce) using the empirical discriminant of Macdonald et al. (2009) (Fig. 7). The phase is very homogeneous, e.g. TiO<sub>2</sub> varies in the range 15.25–15.67 wt.%. The average composition, on the basis of 22 oxygens and with all Fe calculated as Fe<sup>2+</sup>, can be expressed as (Ce<sub>1.63</sub>La<sub>1.29</sub>Ca<sub>0.65</sub>Nd<sub>0.23</sub>Th<sub>0.14</sub>Pr<sub>0.11</sub>)<sub>3.91</sub>Fe<sup>2+</sup>(Fe<sup>2+</sup><sub>1.01</sub>Ti<sub>0.53</sub>Nb<sub>0.21</sub>Mn<sub>0.17</sub>Mg<sub>0.07</sub>Al<sub>0.05</sub>)<sub>2.04</sub>Ti<sub>2.00</sub>(Si<sub>2</sub>O<sub>7</sub>)<sub>2</sub>O<sub>8</sub>, which fits well with the standard formula for the chevkinite group, A<sub>4</sub>BC<sub>2</sub>D<sub>2</sub>(Si<sub>2</sub>O<sub>7</sub>)<sub>2</sub>O<sub>8</sub>.

Compositions of the altered chevkinite (Zone B) are given in Table 1 and Supplementary Table 1a. Compared to the unaltered chevkinite-(Ce), the phase has elevated Ti, Th, Nb, Zr, Al and Ba, and lower LREE, Fe, Ca, Mn and Sr. It has low oxide totals (80.13–94.40 wt.%; average 88.61 wt.%), low cation sums in the A and B sites and low sums of cations (11.57–12.82 apfu; average 11.86 apfu). It is impossible to fit the compositions satisfactorily into the standard chevkinite



**Table 6** Representative compositions of ThSiO<sub>4</sub> in K4

	1	2	3	4	5	6	7	8	9	10
wt%										
P <sub>2</sub> O <sub>5</sub>	5.17	1.02	1.17	0.86	0.32	0.90	0.17	1.22	0.88	1.17
SiO <sub>2</sub>	14.34	17.69	16.17	17.17	14.00	5.82	15.99	16.50	13.30	12.64
TiO <sub>2</sub>	0.12	0.10	0.05	0.05	0.38	2.05	0.16	0.14	bd	0.07
ThO <sub>2</sub>	63.01	61.31	70.41	63.00	71.89	60.47	72.09	61.75	68.24	68.70
UO <sub>2</sub>	0.79	0.84	0.67	0.53	0.75	0.55	0.67	0.78	0.65	0.70
Al <sub>2</sub> O <sub>3</sub>	bd	bd	bd	bd	0.18	0.17	0.28	0.02	0.09	0.10
Y <sub>2</sub> O <sub>3</sub>	bd	bd	bd	bd	0.25	bd	0.42	bd	0.37	0.66
La <sub>2</sub> O <sub>3</sub>	4.75	2.77	2.11	1.63	0.26	2.50	bd	2.73	0.33	0.47
Ce <sub>2</sub> O <sub>3</sub>	6.77	3.48	2.69	2.37	0.25	2.83	0.27	3.83	0.88	1.07
Pr <sub>2</sub> O <sub>3</sub>	bd	0.55	0.58	bd	0.37	bd	0.15	0.16	0.26	bd
Nd <sub>2</sub> O <sub>3</sub>	1.00	0.75	0.53	0.36	bd	0.63	0.23	0.79	0.28	0.39
Sm <sub>2</sub> O <sub>3</sub>	bd	bd	0.53	0.36	bd	bd	bd	bd	0.51	bd
Gd <sub>2</sub> O <sub>3</sub>	bd	bd	bd	0.33	bd	0.31	bd	bd	bd	0.47
CaO	0.52	1.80	1.04	2.20	1.35	1.96	1.22	1.48	1.56	1.77
MnO	0.06	0.16	bd	0.31	bd	bd	bd	0.20	bd	bd
FeO*	0.11	1.45	1.34	1.47	0.60	3.89	0.56	3.78	0.79	0.41
PbO	0.60	bd	bd	bd	bd	bd	bd	0.28	bd	bd
F	bd	bd	0.39	0.38	0.47	0.89	0.59	bd	0.36	0.38
Sum	97.24	91.92	97.68	91.02	91.07	82.97	92.80	93.66	88.50	89.00
O = F	0.00	0.00	0.16	0.16	0.20	0.37	0.25	0.00	0.15	0.16
Total	97.24	91.92	97.52	90.86	90.87	82.60	92.55	93.66	88.35	88.84
Formulae on basis of 4 oxygens										
Th	0.749	0.761	0.871	0.793	0.996	1.009	0.950	0.766	0.967	0.976
U	0.009	0.010	0.008	0.007	0.010	0.009	0.009	0.009	0.009	0.010
Pb	0.008	0.000	0.000	0.000	0.000	0.000	0.000	0.004	0.000	0.000
P	0.229	0.047	0.054	0.040	0.016	0.056	0.008	0.056	0.046	0.062
La	0.092	0.056	0.042	0.033	0.006	0.068	0.000	0.055	0.008	0.011
Ce	0.129	0.069	0.054	0.048	0.006	0.076	0.006	0.076	0.020	0.024
Pr	0.000	0.011	0.011	0.000	0.008	0.000	0.003	0.003	0.006	0.000
Nd	0.019	0.015	0.010	0.007	0.000	0.016	0.005	0.015	0.006	0.009
Sm	0.000	0.000	0.010	0.007	0.000	0.000	0.000	0.000	0.011	0.000
Gd	0.000	0.000	0.000	0.006	0.000	0.008	0.000	0.000	0.000	0.010
Y	0.000	0.000	0.000	0.000	0.008	0.000	0.013	0.000	0.012	0.022
Ca	0.029	0.105	0.061	0.130	0.088	0.154	0.076	0.086	0.104	0.118
Ti	0.005	0.004	0.002	0.002	0.017	0.113	0.007	0.006	0.000	0.003
Fe <sup>2+</sup>	0.005	0.066	0.061	0.068	0.031	0.238	0.027	0.172	0.041	0.021
Mn	0.003	0.007	0.000	0.015	0.000	0.000	0.000	0.009	0.000	0.000
Al	0.000	0.000	0.000	0.000	0.000	0.000	0.000	0.000	0.000	0.000
Si	0.749	0.964	0.879	0.949	0.853	0.426	0.926	0.900	0.828	0.789
F	0.000	0.000	0.067	0.066	0.091	0.206	0.108	0.000	0.071	0.075
Σ cations	2.03	2.12	2.06	2.11	2.07	2.07	2.07	2.07	2.07	2.07

Descriptions: 1, round grain in chevkinite-(Ce) (42×28 μm); 2, elongate grain in chevkinite-(Ce) (70×14 μm); 3, 4, patchily zoned porous grain (145×45 μm); 5, 6, patchily zoned, partly resorbed crystal (120×50 μm); 7, anhedral grain (70×45 μm); 8, porous anhedral grain (50×30 μm); 9, 10, core and rim of partly resorbed plate (49×38 μm). *FeO\** all Fe as Fe<sup>2+</sup>, *bd* below detection

formula, as shown by the average composition: ((Ce<sub>0.61</sub>Ca<sub>0.48</sub>Th<sub>0.31</sub>La<sub>0.13</sub>Ba<sub>0.10</sub>Nd<sub>0.05</sub>)<sub>1.68</sub>Fe<sup>2+</sup><sub>0.79</sub>(Ti<sub>3.04</sub>Nb<sub>0.43</sub>-Al<sub>0.11</sub>Mg<sub>0.08</sub>Fe<sup>2+</sup><sub>0.06</sub>Zr<sub>0.06</sub>)<sub>3.78</sub>Ti<sub>2.00</sub>(Si<sub>1.82</sub>O<sub>7</sub>)<sub>2</sub>O<sub>8</sub>) There has

been a major loss of La relative to the other LREE, e.g. average La/Ce atomic ratios are 0.79 and 0.22 in unaltered and altered types, respectively.

**Table 7** Compositions of niobian rutile in K4

	1	2	3	4	5	6	7	8	9	10
wt%										
Nb <sub>2</sub> O <sub>5</sub>	6.50	10.33	10.03	4.91	9.71	5.69	11.59	7.71	7.99	10.31
SiO <sub>2</sub>	0.63	0.51	0.54	0.83	0.46	0.16	0.08	1.32	0.53	0.65
TiO <sub>2</sub>	88.20	85.87	86.06	89.70	85.90	87.01	80.19	86.11	87.30	80.37
ZrO <sub>2</sub>	bd	0.14	0.14	bd	0.12	bd	0.93	bd	bd	0.28
Al <sub>2</sub> O <sub>3</sub>	0.10	0.06	0.04	0.24	0.08	0.19	bd	0.43	0.09	0.08
Cr <sub>2</sub> O <sub>3</sub>	0.07	0.05	0.04	0.04	0.03	bd	0.26	0.03	0.03	0.19
MgO	bd	0.04	bd	bd	0.03	bd	bd	0.05	0.03	0.03
CaO	0.08	0.08	0.14	0.14	0.09	0.32	0.05	0.11	0.13	0.16
FeO*	2.61	1.67	1.50	2.12	1.53	1.13	3.99	1.87	1.34	3.13
MnO	bd	bd	bd	0.08	bd	bd	bd	0.09	0.07	0.17
Total	98.19	98.75	98.49	98.06	97.95	94.50	97.09	97.72	97.51	95.37
Formulae on the basis of 2 oxygens										
Nb	0.041	0.065	0.063	0.031	0.061	0.037	0.076	0.049	0.051	0.068
Si	0.009	0.007	0.008	0.011	0.006	0.002	0.001	0.018	0.007	0.009
Ti	0.923	0.899	0.902	0.933	0.905	0.940	0.871	0.903	0.919	0.879
Al	0.002	0.001	0.001	0.004	0.001	0.003	0.000	0.007	0.001	0.001
Zr	0.000	0.001	0.001	0.000	0.001	0.000	0.007	0.000	0.000	0.002
Cr	0.001	0.001	0.000	0.000	0.000	0.000	0.003	0.000	0.000	0.002
Mg	0.000	0.001	0.000	0.000	0.001	0.000	0.000	0.001	0.001	0.001
Ca	0.001	0.001	0.002	0.002	0.001	0.005	0.001	0.002	0.002	0.002
Fe <sup>2+</sup>	0.030	0.019	0.017	0.025	0.018	0.014	0.048	0.022	0.016	0.038
Mn	0.000	0.000	0.000	0.001	0.000	0.000	0.000	0.001	0.001	0.002
Σ cations	1.01	0.99	0.99	1.01	0.99	1.00	1.01	1.00	1.00	1.01

All analyses from anhedral grains in coarser area in Zone C1. Largest grain is 23×9 μm. FeO\* all Fe as Fe<sup>2+</sup>, bd below detection

### Bastnäsité-(Ce)

Representative analyses of REE-carbonates are given in Table 2 and the full data set in Supplementary Table 1b. The dominant REE-carbonate in Zone C2 is bastnäsité-(Ce) with modest Th (≤0.022 apfu) and low Ca (≤0.034 apfu) contents. Fluorine values range from 0.94 to 1.11 apfu, close to the maximum for the site, 1 apfu. The darker areas in the zoned crystals (Fig. 3d) have higher Ca and Th contents than the brighter patches. The REE-carbonate in Zone C1 is also bastnäsité-(Ce), with small amounts of hydroxyl (≤0.064 apfu). It has higher levels of Ca (≤0.092 apfu) and Th (≤0.077 apfu) than the Zone C2 crystals.

The small anhedral grains with lower intensity concentrated towards the outer rims of the alteration crust (Fig. 5a) are considerably more calcic than the main REE-carbonate, with Ca ≤0.25 apfu; they also have a larger OH content, up to 0.40 apfu. It is possible that this phase is a fine intergrowth of bastnäsité and parisité (CaREE<sub>2</sub>(CO<sub>3</sub>)<sub>3</sub>F<sub>2</sub>), the texture not being detectable by SEM imaging. An unusual subhedral grain (~200 μm across) at the rim shows a medium-Z bastnäsité-(Ce) containing trails and patches of a higher-Z

material with Th up to 0.24 apfu (Fig. 5b). Overall, the entry of Th into the REE-carbonates seems to be matched by Ca via the substitution Th<sup>4+</sup> + Ca<sup>2+</sup>=2REE<sup>3+</sup> (Fig. 8), as found by Johan and Johan (2005) in bastnäsité-(Ce) from the Cínovec granite cupola, Czech Republic. Chondrite normalised REE patterns age given in Fig. 9.

### Ilmenite

The FeTi-oxide associated with columbite-(Fe) and bastnäsité-(Ce) in Zone C2 is ilmenite (X<sub>ilm</sub> ~100 %), with minor amounts of Mn (≤0.04 apfu) (Table 3; Supplementary Table 1c). The ilmenite near the contact between Zones C1 and C2, i.e. in the same area as the niobian rutile, and in veins cutting the altered chevkinite has variable, but higher, Mn contents (≤0.52 apfu; ≤22.42 wt.% MnO). They also show impossibly high X<sub>ilm</sub> values up to 110. The anomalous analyses represent the phase “ferropseudobrookite” (Fe<sup>2+</sup>Ti<sup>4+</sup><sub>2</sub>O<sub>3</sub>), which Sakoma and Martin (2002) reported as forming by oxidation of ilmenite in a syenitic aplite dyke of the Tibchi complex, Kalato, Nigeria. They suggested that the “ferropseudobrookite” was stabilised by the incorporation of

**Table 8** Representative analyses of Nb-rich phases

	1	2	3	4	5	6	7	8
wt.%								
WO <sub>3</sub>							0.78	0.96
P <sub>2</sub> O <sub>5</sub>					0.21	0.46		
Nb <sub>2</sub> O <sub>5</sub>	66.79	66.29	32.97	31.02	20.93	12.37	18.17	17.15
Ta <sub>2</sub> O <sub>5</sub>					0.99	bd	0.07	bd
SiO <sub>2</sub>	bd	bd	6.51	1.70	14.52	10.25	10.94	15.86
TiO <sub>2</sub>	3.43	3.49	15.14	20.72	5.80	7.42	3.76	4.19
ZrO <sub>2</sub>	bd	bd	bd	bd	6.80	3.38	1.31	1.25
ThO <sub>2</sub>	bd	bd	18.58	10.74	30.59	30.03	40.28	34.82
UO <sub>2</sub>	bd	bd	bd	bd	0.16	bd	0.25	0.32
Al <sub>2</sub> O <sub>3</sub>					0.33	0.42	0.53	1.11
Y <sub>2</sub> O <sub>3</sub>	bd	bd	1.12	2.17				
La <sub>2</sub> O <sub>3</sub>	0.28	bd	0.99	1.48	0.41	3.91	0.61	0.46
Ce <sub>2</sub> O <sub>3</sub>	0.77	0.58	7.05	9.97	0.79	5.84	0.99	0.79
Pr <sub>2</sub> O <sub>3</sub>	bd	bd	bd	1.31	bd	bd	bd	bd
Nd <sub>2</sub> O <sub>3</sub>	bd	bd	3.65	5.44	0.18	0.61	bd	0.29
Sm <sub>2</sub> O <sub>3</sub>	bd	bd	0.60	0.54	bd	bd	bd	bd
Gd <sub>2</sub> O <sub>3</sub>	bd	bd	0.80	1.28	bd	bd	bd	bd
MgO					0.13	0.10	0.10	0.17
CaO	15.04	14.76	2.08	2.65	1.43	1.49	1.30	1.20
FeO*	0.31	bd	1.34	2.40	1.78	3.08	2.91	5.46
MnO	bd	bd	0.81	bd	0.08	0.37	0.09	0.09
SrO	3.52	3.59	0.52	bd	0.25	0.43		
BaO	bd	bd	2.73	0.29	0.59	0.30	0.25	0.16
Na <sub>2</sub> O	7.28	7.48	bd	0.08	bd	bd	bd	bd
F	5.22	5.64	bd	bd	bd	0.37		
Sum	102.64	101.83	94.89	91.79	80.30	72.58	81.56	83.32
O = F	2.20	2.37	0.00	0.00	0.00	0.16		
Total	100.44	99.46	94.89	91.79	80.30	72.42	81.56	83.32

Explanation: 1, 2, in anhedral grain intergrown with quartz (Fig. 6a); 3–4, in band rimming Zone C (Fig. 6c); 5, 6, in interstitial wedge, Zone C1 (Fig. 6b); 7, 8, associated with symplectites, Zone C1

FeO\* all Fe as Fe<sup>2+</sup>, bd below detection, Blank, not determined

Nb, Ta and Si. Several point analyses in the contact zone between Zones B and C are indeed Nb-rich ( $\leq 8.06$  wt.% Nb<sub>2</sub>O<sub>5</sub>).

### Columbite-(Fe)

The general formula for minerals of the columbite group is  $AB_2O_6$ , where  $A = Fe^{2+}$ , Mn, Mg and  $B = Nb$ , Ta. Minor amounts of Fe<sup>3+</sup>, Sc, Ti, Sn and W are common. Electron microprobe data for columbite in K4 are given in Table 4 and Supplementary Table 2a. Oxide totals are in the range 98.18–100.18 wt.% (average 98.93 wt.%) and the cation sums, calculated on the basis of 6 oxygens, range from 2.99 to 3.02 apfu (average 3.00 apfu). Both Fe- and Mn-dominant

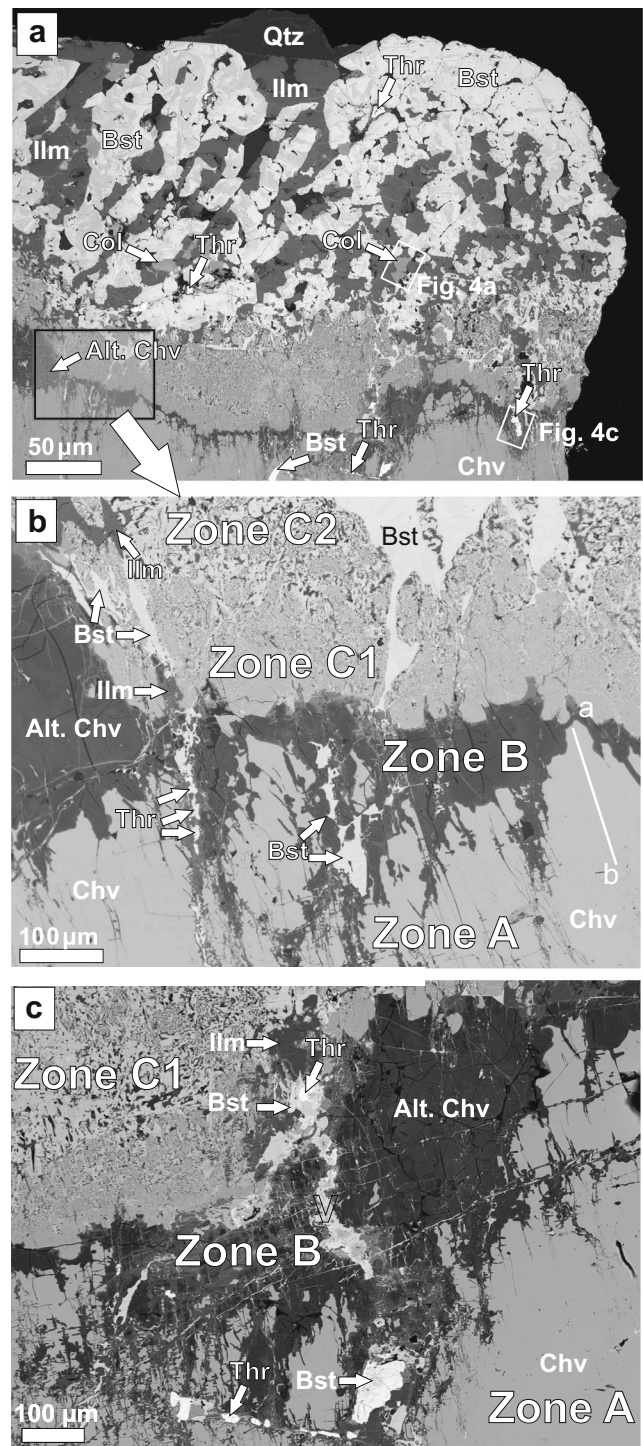
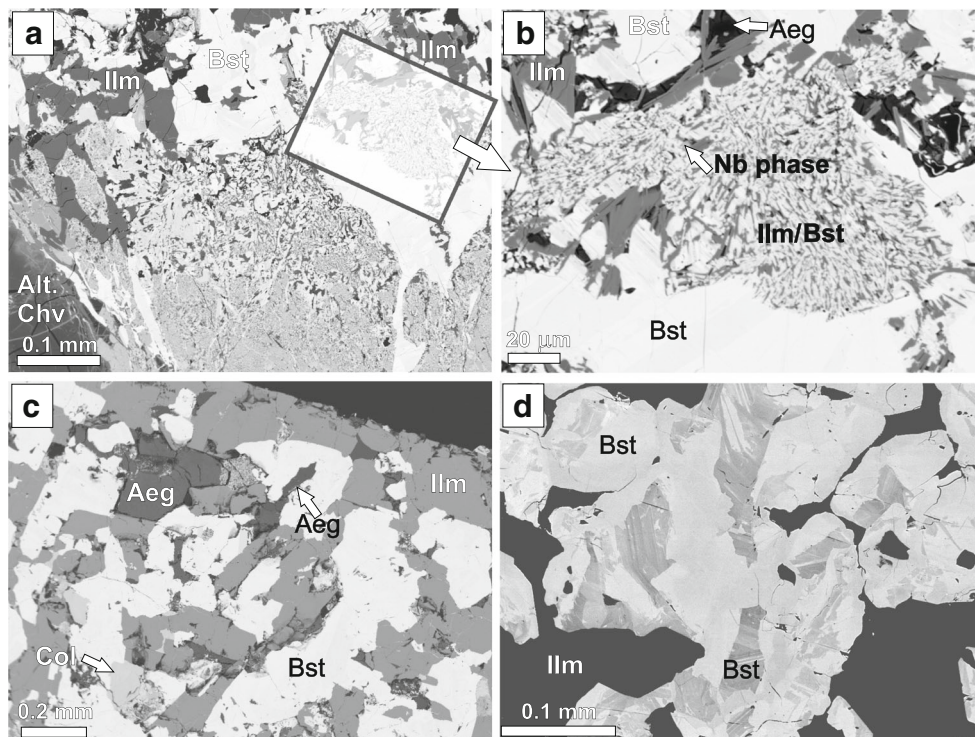


**Fig. 2** a More detailed (inverted) BSE image of the lower left part of Fig. 1b, with the main phases labelled: Bst, bastnäsite-(Ce); Col, columbite-(Fe); Ilm, ilmenite; Qtz, quartz; Thr, ThSiO<sub>4</sub>. Note, in particular, the textural complexity of the area between Zones C1 and C2. b BSE image of the relationships between Zones A, B and C. Analyses made along the profile a-b marked in the chevkinite-(Ce) are presented in Supplementary Table 1a. c This BSE image stresses the complexity of the relationships shown in Fig. 2b

types are present but since the average Fe and Mn values are 0.46 and 0.45 apfu, respectively, we refer to the phase in

**Fig. 3** BSE images showing, **a** Transition from Zone C1 to C2, showing the large increase in grain size. The coarser area includes small patches of the finer-grained material. **b** Symplectite texture composed of an intergrowth of ilmenite and bastnasite-(Ce). A small grey grain of a Nb-rich phase is also seen. **c** Zone C2 is an interlocking mosaic of ilmenite, bastnäsite-(Ce), columbite-(Fe) and quartz (not seen on this image). The darkest phase is aegirine (Aeg). **d** Zoning in bastnäsite-(Ce)



general as columbite-(Fe). The phase contains significant levels of  $\text{TiO}_2$  (1.73–4.06 wt.%; 0.075–0.106 apfu), indicating modest solid solution towards rutile,  $\text{Sc}_2\text{O}_3$  (0.25–0.53 wt.%),  $\text{WO}_3$  (0.48–2.31 wt.%) and  $\text{MgO}$  ( $\leq 0.07$  wt.%). The contents of  $\text{REE}_2\text{O}_3$  (0.15–

3.32 wt.%) are unusually high, judging from general studies of columbite composition by Ercit et al. (1995) and Wise et al. (1998).

Zonation in the columbite takes two forms, oscillatory and patchy (Fig. 4). Oscillatory zoning in columbite is most

**Fig. 4** **a** Zoning in columbite-(Fe). The upper fragment has a fairly homogeneous darker core; the remainder of the crystal is a patchy intergrowth of darker and lighter components, the lighter apparently of later formation (and see the light veinlet in the dark core). **b** Oscillatory zoning in the upper left part of this columbite-(Fe) has been truncated by a patchy darker material, in turn cut by a lighter vein. **c** Partly resorbed, fractured  $\text{ThSiO}_4$  with patchy zonation and a porosity which is most fully developed in the darker zones. **d** Patchily zoned, originally prismatic,  $\text{ThSiO}_4$  containing abundant pores (arrowed)

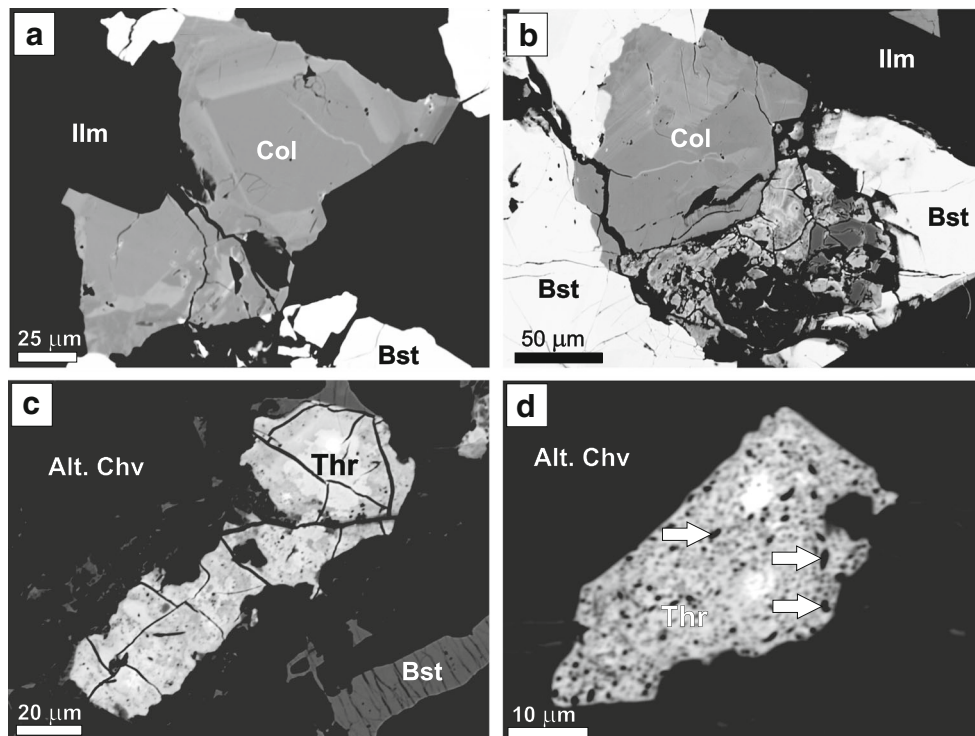
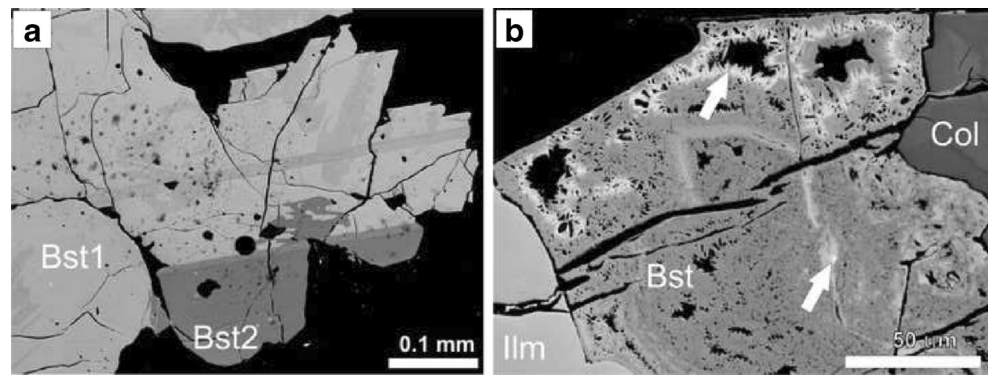


**Fig. 5** **a** A darker REE-carbonate (Bst2) has a sharp contact with, and partially penetrates, bastnäsite-(Ce) (Bst1) at the rim of the alteration crust (Zone C). **b** A REE-carbonate crystal, in contact with columbite-(Fe) and ilmenite, is veined by a more Th-rich carbonate which also forms small tooth-shaped crystals lining vug-like holes (arrowed)



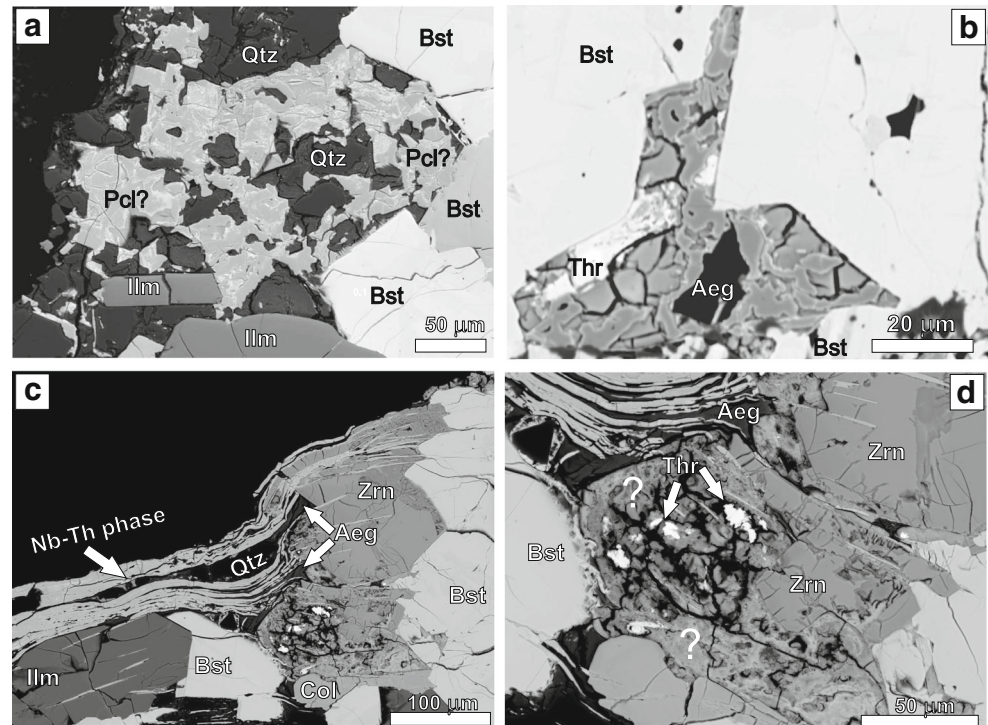
commonly found in granites and pegmatites (Abdalla et al. 1998; Lahti 2000; Tindle and Breaks 2000; Rao et al. 2009; Wise and Brown 2011) and is taken to be a primary crystallization texture. Patchy zoning, as exemplified in Fig. 4b, has been reported by Lahti (1987, 2000), Abdalla et al. (1998), Tindle and Breaks (2000) and Wise and Brown (2011) and is usually ascribed to hydrothermal alteration of the columbite. Compositional variation in both types of zoning can be broadly expressed as  $(\text{Fe}^{2+} + \text{Nb}^{5+} + \text{W}^{6+}) \leftrightarrow (\text{REE}^{3+} + \text{Th}^{4+} + \text{Ti}^{4+} + \text{Mn}^{2+})$  (Fig. 10).

### Aegirine

Aegirine in the main alteration rim has the composition  $\text{Na}_{0.94}\text{Ca}_{0.06}\text{Fe}^{3+}_{0.90}\text{Mg}_{0.03}\text{Si}_{2.02}\text{O}_6$ . From its textural relationships with the bastnäsite-(Ce) and columbite-(Fe), we

infer that it formed from the hydrothermal fluids. In the majority of cases it has been strongly altered, with addition of significant amounts of Al (5.21–6.26 wt.%  $\text{Al}_2\text{O}_3$ ), almost total removal of Na (to below detection) and decrease of the sum of cations (3.32–3.38 apfu) (Table 5). It is clear from BSE images that at least two phases are contributing to the bulk composition; judging from the morphology and significant Al content it is possible that one at least is a phyllosilicate. The formulae for the altered phase in Table 5 are given for comparison with the unaltered phase; there is no implication that it represents aegirine.

**Fig. 6** **a** A Nb-rich phase, possibly “fluorcalciopyrochlore”, replaces quartz in a complex composite grain at the rim of the alteration crust. **b** Complex intergrowth of unidentified Nb- and Th-bearing phases in Zone C. The wedge also contains altered  $\text{ThSiO}_4$  and altered aegirine. **c** The rim of the alteration crust is locally rimmed by a thin band of an unidentified Nb-rich phase which has replaced quartz. The phase veins zircon and ilmenite crystals. **d** Blow-up of the central part of Fig. 6c. Bright grains of  $\text{ThSiO}_4$  are included in an unidentified Th-rich phase (?) apparently altered to a complex mix of components of different intensities



### $\text{ThSiO}_4$

Representative analyses of  $\text{ThSiO}_4$  are given in Table 6 and the full data set in Supplementary Table 2b. Oxide totals are

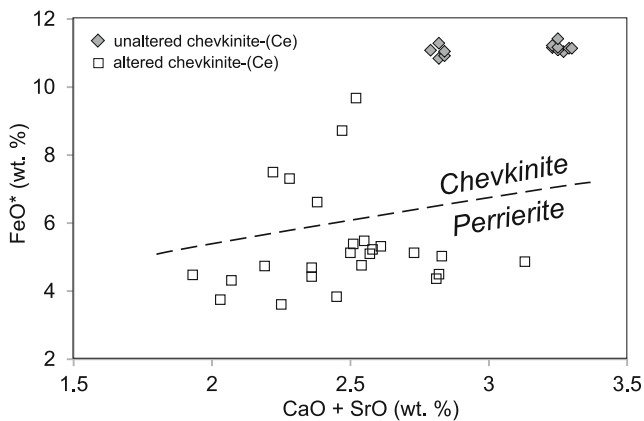


**Fig. 7** Empirical discrimination plot of chevkinite and perrierite (Macdonald et al. 2009). The unaltered chevkinite-(Ce) plots in the chevkinite field, whereas the altered chevkinite spreads into the perrierite field. Data from Supplementary Table 1a

low, 82.60–97.24 wt.%, and the cation sums are high (2.03–2.39 apfu), clear indicators that the mineral has been significantly altered. SiO<sub>2</sub> levels are as low as 5.51 wt.%, raising doubts that the material is, or was, crystalline but was perhaps derived from an amorphous gel. The abundances of certain non-formula elements are high: P<sub>2</sub>O<sub>5</sub> ≤ 8.24 wt.%, CaO ≤ 3.02 wt.%, ΣREE<sub>2</sub>O<sub>3</sub> ≤ 22.44 wt.%; FeO\* 4.05 wt.%, and TiO<sub>2</sub> ≤ 2.05 wt.%, the REE being dominated by the LREE. These elements are known to be incorporated into ThSiO<sub>4</sub> during interaction with hydrothermal fluids (Lumpkin and Chakoumakos 1988; Pointer et al. 1988; Johan and Johan 2005; Förster 2006; Berger et al. 2008; Uher et al. 2009; Soman et al. 2010; Piilonen et al. 2013). The proportion of

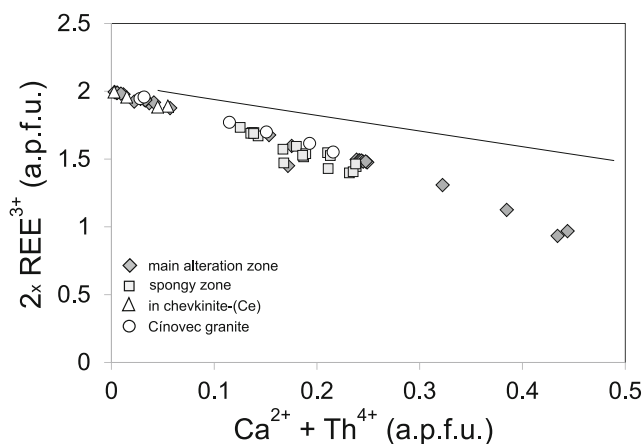


**Fig. 8** Possible coupled substitution scheme for bastnäsite-(Ce). The phase in Zone C1 tends to have higher Ca and Th than crystals in the main part of Zone C. Analyses with (Ca+Th) > 0.3 are from the higher Z material in the Th-rich grain shown in Fig. 5b. Data from Supplementary Table 1b. Compositions of bastnäsite-(Ce) from the Cinovec granite cupola, Czech Republic, are given for comparison (Johan and Johan 2005). The location of the majority of analyses below the  $x + y = 2$  line may partly be due to the presence of MREE and HREE just below the limit of detection of the electron microprobe technique

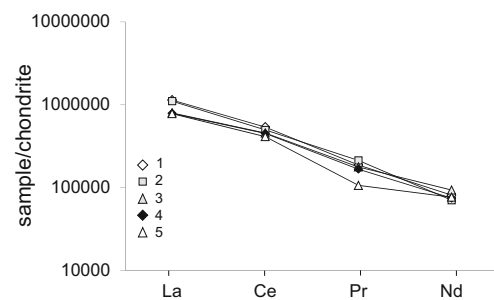


**Fig. 9** Chondrite-normalised LREE patterns for bastnäsite-(Ce). Patterns 1 and 2 are from Zone C2 (Table 2, nos. 1, 2); pattern 3 from darker, more calcic phase at rim (Table 2, no. 5; Fig. 5b); pattern 4, lighter vein in Th-rich crystal (Table 2, no. 7; Fig. 5b); pattern 5, in Zone C1 (Table 2, no. 8). Normalising factors from Sun and McDonough (1989)

OH in the formulae was calculated from charge balance and ranged from 0.0 to 2.4 (Supplementary Table 2b).

As shown on a REE-Ca-Fe plot (Fig. 11), there are large variations within individual crystals and major overlaps between ThSiO<sub>4</sub> phases from Zones A and B. ThSiO<sub>4</sub> from Zone C2 plots, however, nearer the REE-Ca sideline than those from the other zones. It appears that incorporation of the non-formula elements into the ThSiO<sub>4</sub> was heavily dependent on the local conditions, especially rapid variations in the composition of the fluid phase(s).

### Nb-bearing phases

Compositions of niobian rutile are given in Table 7. The main variations are in Ti, Nb and Fe contents and the compositional range is from Ti<sub>0.87</sub>Nb<sub>0.08</sub>Fe<sub>0.05</sub> to Ti<sub>0.94</sub>Nb<sub>0.04</sub>Fe<sub>0.01</sub>.

Compositions of the other Nb-bearing phases are presented in Table 8 and Supplementary Table 3a. The phase replacing quartz (Fig. 6a) and described above as “homogeneous grey” contains high levels of Nb<sub>2</sub>O<sub>5</sub> (63.8–66.79 wt.%), CaO (14.56–15.04 wt.%), Na<sub>2</sub>O (7.02–7.48 wt.%), SrO (3.25–3.59 wt.%) and F (5.22–5.64 wt.%). The average compositions at the *A* and *B* sites, on the basis of *B* cations = 2, are Ca<sub>0.98</sub>Na<sub>0.87</sub>Sr<sub>0.13</sub> apfu and Nb<sub>1.83</sub>Ti<sub>0.16</sub> apfu, respectively.

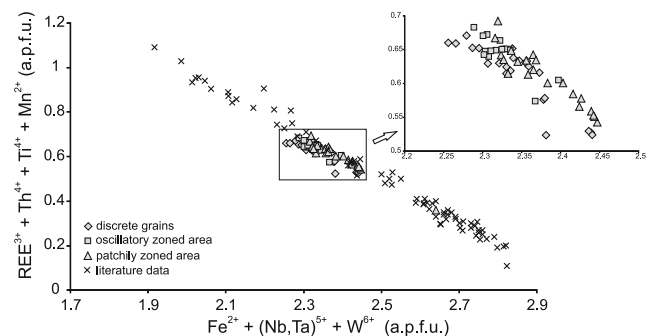


**Fig. 10** Possible coupled substitution scheme for columbite. The oscillatory and patchily zoned areas are in the same crystal (Fig. 4b). Data from Supplementary Table 2a. Literature data from Lahti (1987), Abdalla et al. (1998), Tindle and Breaks (2000) and Wise and Brown (2011)

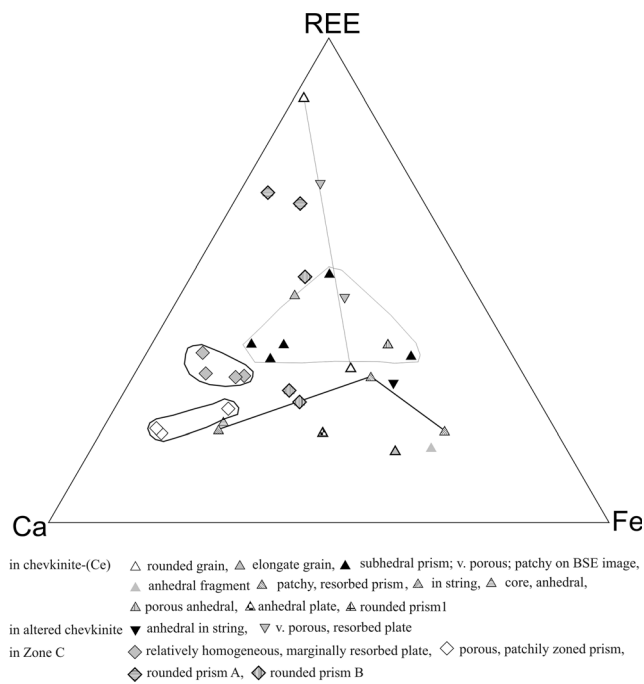
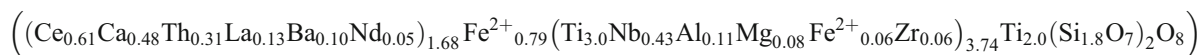


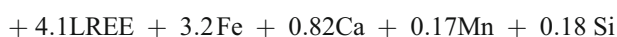
**Fig. 11** Relative proportions of REE-Ca-Fe in ThSiO<sub>4</sub>. There are no simple correlations between the elements and there are large ranges even in single crystals (shown as selected fields or connected by solid lines). ThSiO<sub>4</sub> from Zone C2 tends to have higher Ca than those from Zones A and B. Data from Supplementary Table 2b

The content of F is 1.07 apfu. The phase belongs to the pyrochlore supergroup and following recommendations in Atencio et al. (2010), it is cautiously termed “fluorcalciopyrochlore” here. The two other components are compositionally slightly different, with variable proportions of Nb, Th, Na and Ca.

The thin band forming the outer rim of the alteration crust (Fig. 6c) has high contents of Nb<sub>2</sub>O<sub>5</sub> (31.02–32.97 wt.%) and TiO<sub>2</sub> (15.14–22.01 wt.%), and high but variable ThO<sub>2</sub> contents (5.81–18.58 wt.%). Abundances of BaO, REE<sub>2</sub>O<sub>3</sub> and SiO<sub>2</sub> are also very variable. The analytical totals are low, 91.79–94.89 wt.%, and the phase is clearly strongly altered.



altered chevkinite



The development of the main alteration rim began with the formation of Zone C1 rimming Zone B. As the rim developed, crystal size increased. A particularly complex zone occurs immediately before Zone C2, where there was local

The phase (or phases) in the interstitial wedge (Fig. 6b) and symplectites (Fig. 3b) contains high ThO<sub>2</sub> (22.35–40.28 wt.%) and Nb<sub>2</sub>O<sub>5</sub> (10.93–20.93 wt.%) and moderately high and variable abundances of SiO<sub>2</sub> (10.25–15.86 wt.%), ZrO<sub>2</sub> (1.31–10.74 wt.%) and TiO<sub>2</sub> (3.76–7.42 wt.%). One phase in the wedge has high Nb<sub>2</sub>O<sub>5</sub> (65.07 wt.%), CaO (13.71 wt.% and F (2.32 wt.%) and low ThO<sub>2</sub> (0.71 wt.%) and may be a member of the pyrochlore supergroup. It is not clear as to which mineral species the other phases belong; if, however, they formed from gels, as suggested above, they cannot be considered as mineral species.

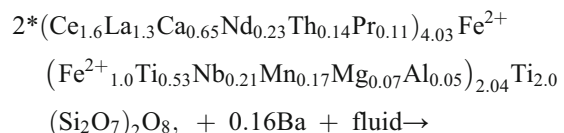
Whilst many important textural, compositional and structural features of the Nb-rich phases are as yet unknown, the point to be stressed is that they provide evidence of the mobility of Nb and Th in the latest stages of the alteration process. It is suggested below that the Nb may have been released by alteration of columbite.

## Discussion

### Sequence of events

We infer the following stages in what was essentially a continuous replacement process (Fig. 12).

Hydrothermal alteration of chevkinite-(Ce) released LREE, Fe, Ca and Mn and concentrated 4- and 5-valent cations (Ti, Th, Zr, Nb) in the residual, altered chevkinite, phase.



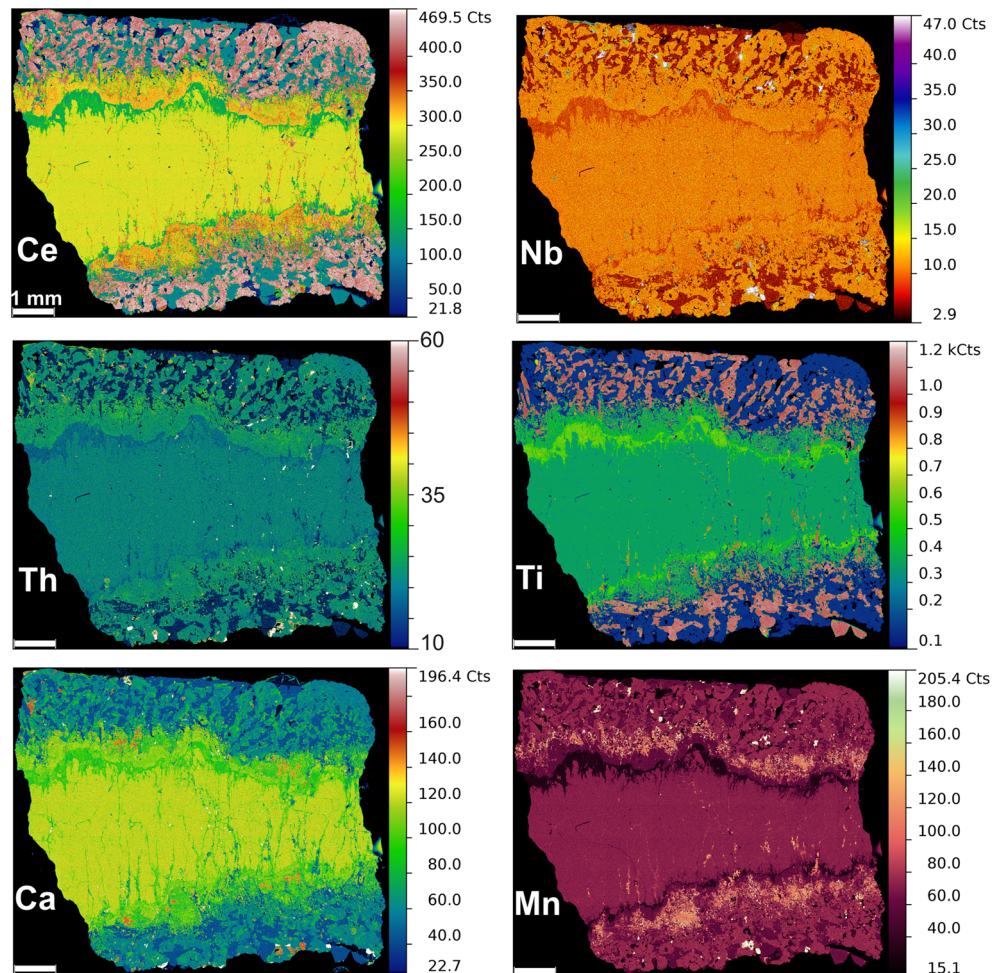
chevkinite-(Ce)

development of symplectites comprising intergrowths of Mn-rich ilmenite and bastnäsite-(Ce) and rapid variations in grain size and texture (Figs. 2 and 3). Niobian rutile and ferropseudobrookite occur in coarser areas. These features possibly reflect the kinetics of the replacement process, Zone C2 being a product of the recrystallization of Zone C1. The recrystallization was accompanied by an increase in the grain





**Fig. 13** Element distribution maps covering the thin section shown in Fig. 1b



### Rare earth elements

The behaviour of the REE during alteration of the chevkinite-(Ce) was complex. Formation of the altered chevkinite zone released significant proportions of LREE, as exemplified by Ce on Fig. 13. The selective mobility of La relative to the other LREE may have reflected the high alkalinity of the fluids. The REE were tied up in the bastnäsite-(Ce) in Zone C1 and then in bastnäsite-(Ce) in Zone C2. At that stage, significant amounts of REE also entered  $\text{ThSiO}_4$ , the proportions being highly variable, e.g.  $[\text{La}/\text{Y}]_{\text{CN}}$  ranges from  $\sim 1$  to 50. The absence of any secondary La-dominant phase suggests that at least part of the La was transported out of the system by fluids.

### Iron and manganese

Iron was depleted in the altered chevkinite and mainly partitioned into ilmenite and columbite-(Fe) in Zone C2. Late-stage ilmenite-bearing veinlets occur in the

chevkinite-(Ce). Manganese makes some interesting contrasts with Fe. In particular, the Mn-rich ilmenite in the part of Zone C2 just above Zone C1 stands out as distinct, speckled, light areas and the columbite-(Fe) forms white spots in Zone C2 (Fig. 13).

### Calcium

The Ca element distribution map (Fig. 13) shows in particular the incipient alteration along fractures in the chevkinite-(Ce). It also shows the patchy distribution of the calcic bastnäsite-(Ce) (red spots), interpreted here as a late replacement of the bastnäsite-(Ce).

### Nature of the hydrothermal fluids

The formation of abundant bastnäsite-(Ce) is *a priori* evidence that the fluids were very  $\text{CO}_2$ -rich. The high F content of the carbonate in Zone C2 points also to a

high F content in the fluids. The higher levels of Ca and (inferred) OH in the bastnäsite-(Ce) in Zone C1 may indicate that the activity of F was lower and that of water higher, at least locally, during that stage. In the latest stages, the formation of the calcic bastnäsite-(Ce) signalled a return to slightly higher Ca and water activities. The fluid also contained small quantities of P, now incorporated into the rare monazite-(Ce). It was noted above that there was formation of abundant apatite during the earlier carbonatization of the pegmatites; in contrast, the P contents of the fluids altering the aegirine-microcline pegmatite were unusually low. There is no evidence for significant Cl or S components in the fluids.

Some, rather contradictory, evidence as to the  $fO_2$  of the fluids is given by the FeTi-oxides. It has been shown experimentally (Lindsley 1991) and empirically (Sakoma and Martin 2002) that rutile, hematite and 'ferropseudobrookite' form in primary ilmenite through oxidation-induced exsolution. The calculated ilmenite-rutile reaction is located between the Ni-NiO and magnetite-hematite buffers (Zhao et al. 1999, and references therein). The presence of niobian rutile in parts of Zone C1 suggests that at that stage the  $fO_2$  was relatively high but did not exceed the magnetite-hematite buffer. In contrast, the high MnO contents ( $\leq 16.82$  wt% MnO) in ilmenite close to the boundary between Zones C1 and C2 might point to lower  $fO_2$  during its formation (Cassidy et al. 1988). A period of lower  $fO_2$  might also have followed the crystallization of aegirine (Markl et al. 2010) and the absence of  $Fe^{3+}$  in the ferropseudobrookite also points to relatively low  $fO_2$ .

### Relationships between CGM composition and nature of accessories

Columbite is a typical product of the hydrothermal alteration of pyrochlore in many carbonatites (including calcite carbonatites of the Vishevy Mts), syenites (including syenite-pegmatites of Vishevy Mts) and alkali granites during the later stages of alteration. As examples, Uher et al. (2009) found columbite-(Fe) forming rare irregular intergrowths with Nb-Ta-rich rutile in the Prašivá granitic pegmatites, Slovakia. Doroshkevich et al. (2009, p.1113) described columbite + quartz replacing pyrochlore in the Amba Dongar carbonatite complex, Gujarat, India, and Lahti (2000, p. 112) recorded pyrochlore-microlite replacing marginal parts of columbite crystals and small columbite-group phases

occurring in pyrochlore samples from granitic pegmatites of the Eräjärvi district, South Finland. René and Škoda (2011) recorded W-enriched columbite-(Fe) forming inclusions in some rutile grains from alkali-feldspar granites of the Krásno-Horní Slavkov ore district, Czech Republic. Sakoma and Martin (2002) described a columbite-(Fe)-ilmenite-'ferropseudobrookite'-rutile assemblage in an aplitic syenite dyke of the Tibchi granite complex, Nigerian Younger Granite igneous province, suggesting crystallization of columbite and primary ilmenite during the magmatic stage and of secondary Mn-rich ilmenite, 'ferropseudobrookite' and rutile during the postmagmatic stages. In K4, the columbite-(Fe) is associated with ilmenite and bastnäsite-(Ce), in what appears to be the first record of this paragenesis. The question arises, What promoted the crystallization of columbite?

In alkaline *magmatic* systems, the solubility of columbite is high, even at low temperatures, and especially when fluxed by F. Linnen and Keppler (1997) suggested that columbite saturation in natural alkaline melts is unlikely and that pyrochlore is more likely to form. The further question arises: why did columbite form rather than Nb,Ti,REE-oxides, rutile or niobian ilmenite? It may be that columbite has very low solubility in  $CO_2$ -rich fluids and that two potential assemblages may be distinguished: 1: ilmenite + columbite + REE-carbonate, and 2: ilmenite + titanite + rutile + Nb-oxides. The first is stabilised by high  $X(CO_2)$  and/or low Ca activity and the second by lower  $X(CO_2)$  and higher Ca activity. A limit to the Ca activity might have been given, however, by reactions of the type:  $2CeCO_3F + CaO = CaF_2 + Ce_2O_3 + CO_2$  (Hsu 1992; Guastoni et al. 2009).

The fact that the chevkinite did not alter to allanite, as commonly described in the alteration of chevkinite, may be ascribed to the loss from the system of much of the Si and Ca, to the scarcity of mobile Al in the system, and possibly also to high  $X(CO_2)$ . The replacement of allanite by REE-carbonates has been described by Berger et al. (2008), Savel'eva and Karmanov (2008) and Papoutsas and Pe-Piper (2013) and is at least consistent with allanite being unstable under conditions of high  $X(CO_2)$ .

**Acknowledgments** We thank Igor Broska and Bartosz Budzyń for very helpful journal reviews and Anton Beran for editorial handling. We also thank Ms Lidia Ježak for assistance in the electron microprobe laboratory. The study was partly supported by grants from the National Science Centre (number N N307 634040), and the Earth Science department of the Russian Academy of Sciences (Program 9) to DZ.

## Appendix

**Table 9** EMP analytical conditions for chevkinite

Element	Line	Crystal	Standard	Approx. detection limit (wt.%)
Al	K $\alpha$	TAP	orthoclase	0.008
Ba	L $\alpha$	LiF	barite	0.114
Ca	K $\alpha$	PET	CaSiO <sub>3</sub>	0.008
Ce	K $\alpha$	PET	CeP <sub>5</sub> O <sub>14</sub>	0.053
Dy	L $\beta$	LiF	REE1	0.312
Eu	L $\beta$	LiF	REE2	0.263
Fe	K $\alpha$	LiF	hematite	0.034
Gd	L $\beta$	LiF	GdP <sub>5</sub> O <sub>14</sub>	0.126
Hf	M $\alpha$	TAP	Hf-SPI	0.033
La	L $\alpha$	PET	LaB <sub>6</sub>	0.052
Mg	K $\alpha$	TAP	diopside	0.006
Mn	K $\alpha$	LiF	rhodonite	0.036
Na	K $\alpha$	TAP	albite	0.012
Nb	L $\alpha$	PET	Nb metal	0.054
Nd	L $\beta$	LiF	NdP <sub>5</sub> O <sub>14</sub>	0.121
P	K $\alpha$	PET	Apatite Jap2	0.014
Pr	L $\beta$	LiF	PrP <sub>5</sub> O <sub>14</sub>	0.119
Sc	K $\alpha$	PET	Sc metal	0.010
Si	K $\alpha$	TAP	CaSiO <sub>3</sub>	0.006
Sm	L $\beta$	LiF	SmP <sub>5</sub> O <sub>14</sub>	0.133
Sr	L $\alpha$	TAP	SrTiO <sub>3</sub>	0.027
Ta	M $\alpha$	TAP	Ta metal	0.036
Tb	L $\alpha$	LiF	REE4	0.144
Th	M $\alpha$	PET	ThO <sub>2</sub> synthetic	0.086
Ti	K $\alpha$	PET	rutile	0.016
U	M $\beta$	PET	vorlanite	0.077
Y	L $\alpha$	TAP	Y <sub>3</sub> Al <sub>5</sub> O <sub>12</sub>	0.028
Yb	L $\alpha$	LiF	REE3	0.136
Zr	L $\alpha$	PET	Zircon ED2	0.051

REE1 to 4: glasses with REE (reference samples of Jarosewich, E. and Boatner L. (1991) Rare-earth element reference samples for electron microprobe analysis. *Geostandards Newsletter*, **15**, 397–399)

**Open Access** This article is distributed under the terms of the Creative Commons Attribution 4.0 International License (<http://creativecommons.org/licenses/by/4.0/>), which permits unrestricted use, distribution, and reproduction in any medium, provided you give appropriate credit to the original author(s) and the source, provide a link to the Creative Commons license, and indicate if changes were made.

## References

- Abdalla HM, Helba HA, Mohamed FH (1998) Chemistry of columbite-tantalite minerals in rare metal granitoids, Eastern Desert, Egypt. *Mineral Mag* 62:821–836
- Atencio D, Andradi MB, Christy AG, Gieré R, Kartashov PM (2010) The pyrochlore supergroup of minerals: nomenclature. *Can Mineral* 48: 673–698
- Bagiński B, Macdonald R, Dzierzanowski P, Zozulya D, Kartashov PM (2015) Hydrothermal alteration of chevkinite-group minerals: products and mechanisms. Part 1. Hydration of chevkinite-(Ce). *Mineral Mag*
- Berger A, Gnos E, Janots E, Fernandez A, Giese J (2008) Formation and composition of rhabdophane, bastnasite and hydrated thorium minerals during alteration: implications for geochronology and low-temperature processes. *Chem Geol* 254:238–248
- Budzyń B, Harlov DE, Williams ML, Jercinovic MJ (2011) Experimental determination of stability relations between monazite, fluorapatite, allanite, and REE-epidote as a function of pressure, temperature, and fluid composition. *Am Mineral* 96:1547–1567

- Cassidy KF, Groves DI, Binns RA (1988) Manganian ilmenite formed during regional metamorphism of Archean mafic and ultramafic rocks from Western Australia. *Can Mineral* 26:999–1012
- Doroshkevich AG, Viladkar SG, Ripp GS, Burtseva MV (2009) Hydrothermal REE mineralization in the Amba Dongar carbonatite complex, Gujarat, India. *Can Mineral* 47:1105–1116
- Ercit TS, Wise MA, Černý P (1995) Compositional and structural systematics of the columbite group. *Am Mineral* 80:613–619
- Es'kova EM, Zhabin AG, Mukhitdinov GN (1964) Mineralogy and geochemistry of rare elements of the Cherry Mountains. Nauka, Moscow, **320 pp. (in Russian)**
- Förster H-J (2006) Composition and origin of intermediate solid solutions in the system thorite-xenotime-zircon-coffinite. *Lithos* 88:35–55
- Guastoni A, Nestola F, Giaretta A (2009) Mineral chemistry and alteration of rare earth element (REE) carbonates from alkaline pegmatites of Mount Malosa, Malawi. *Am Mineral* 94:1216–1222
- Harlov DE, Wirth R, Hetherington CJ (2011) Fluid-mediated partial alteration in monazite: the role of coupled dissolution-precipitation in element redistribution and mass transfer. *Contrib Mineral Petrol* 162:329–348
- Hsu LC (1992) Synthesis and stability of bastnaesites in a part of the system (Ce, La)-F-H-C-O. *Mineral Petrol* 47:87–101
- Jiang N (2006) Hydrothermal alteration of chevkinite-(Ce) in the Shuiquangou syenitic intrusion, northern China. *Chem Geol* 227:100–112
- Johan Z, Johan V (2005) Accessory minerals of the Cínovec (Zinnwald) granite cupola, Czech Republic: indicators of petrogenetic evolution. *Mineral Petrol* 83:113–150
- Kartashov PM (1994) Zr- and Nb-bearing varieties of chevkinite-(Ce) and their alteration products, first occurrence in Mongolia. Ninth IAGOD Symposium, Beijing 2: 696–697
- Lahti SI (1987) Zoning in columbite-tantalite crystals from the granitic pegmatites of the Eräjärvi area, southern Finland. *Geochim Cosmochim Acta* 51:509–517
- Lahti SI (2000) Compositional variation in columbite-group minerals from different types of granitic pegmatites of the Eräjärvi district, South Finland. *J Czech Geol Soc* 45:107–118
- Lindsley DH (1991) Experimental studies of oxide minerals. In: Lindsley DH (ed) *Oxide minerals: petrologic and magnetic significance*. *Revi Mineral* 25:69–106
- Linnen RL, Keppler H (1997) Columbite solubility in granitic melts: consequences for the enrichment and fractionation of Nb and Ta in the Earth's crust. *Contrib Mineral Petrol* 128:213–227
- Lumpkin GR, Chakoumakos BC (1988) Chemistry and radiation effects of thorite-group minerals from the Harding pegmatite, Taos County, New Mexico. *Am Mineral* 73:1405–1419
- Macdonald R, Belkin HE, Wall F, Bagiński B (2009) Compositional variation in the chevkinite group: new data from igneous and metamorphic rocks. *Mineral Mag* 73:777–796
- Macdonald R, Bagiński B, Kartashov P, Zozulya D, Dzierżanowski P (2012) Chevkinite-group minerals from Russia and Mongolia: new compositional data from metasomatites and ore deposits. *Mineral Mag* 76:535–549
- Macdonald R, Bagiński B, Kartashov PM, Zozulya D, Dzierżanowski P (2015) Hydrothermal alteration of chevkinite-group minerals. Part 2. Metasomatite from the Keivy massif, Kola Peninsula, Russia. *Mineral Mag*
- Markl G, Marks M, Frost BR (2010) On the controls of oxygen fugacity in the generation and crystallization of peralkaline melts. *J Petrol* 51:1831–1847
- Nečas D, Klapetek P (2012) Gwyddion: an open-source software for SPM data analysis. *Cent Eur J Phys* 10:181–188
- Oelkers EH, Poitras F (2002) An experimental study of the dissolution stoichiometry and rates of a natural monazite as a function of temperature from 50 to 230 °C and pH from 1.5 to 10. *Chem Geol* 191:73–87
- Papoutsas AD, Pe-Piper G (2013) The relationship between REE-Y-Nb-Th minerals and the evolution of an A-type granite, Wentworth Pluton, Nova Scotia. *Am Mineral* 98:444–462
- Piilonen PC, Rowe R, Poirier G, Grice JD, McDonald AM (2013) Crystal structure determination of a unique Nb-Ti-rich thorite from Mont Saint-Hilaire, Quebec, with comments on 'thorogummite'. *Can Mineral* 51:597–612
- Pointer CM, Ashworth JR, Ixer RA (1988) a) The zircon-thorite mineral group in metasomatized granite, Ririwai, Nigeria 1. Geochemistry and metastable solid solution of thorite and coffinite. *Mineral Petrol* 38:245–262
- Pouchou JL, Pichoir JF (1991) Quantitative analysis of homogeneous or stratified microvolumes applying the model 'PAP'. In: Newbury H (ed) *Electron probe quantitation*. Plenum Press, New York, pp 31–75
- Rao C, Wang RC, Hu H, Zhang WL (2009) Complex internal textures in oxide minerals from the Nanping No. 31 dyke of granitic pegmatite, Fujian Province, southeastern China. *Can Mineral* 47:1195–1212
- René M, Škoda R (2011) Nb-Ta-Ti oxides fractionation in rare-metal granites: Krásno-Horní Slavkov ore district, Czech Republic. *Mineral Petrol* 103:37–48
- Sakoma EM, Martin RF (2002) Oxidation-induced postmagmatic modifications of primary ilmenite, NYG-related aplite dyke, Tibchi granite complex, Kalato, Nigeria. *Mineral Mag* 66:591–604
- Savel'eva VB, Karmanov NS (2008) REE minerals of alkaline metasomatic rocks in the Main Sayan Fault. *Geol Ore Depos* 50:681–696
- Seydoux-Guillaume A-M, Wirth R, Ingrin J (2007) Contrasting response of ThSiO<sub>4</sub> and monazite to natural irradiation. *Eur J Mineral* 19:7–14
- Soman A, Geisler T, Tomaschek F, Grange M, Berndt J (2010) Alteration of crystalline zircon solid solutions: a case study on zircon from an alkaline pegmatite from Zomba-Malosa, Malawi. *Contrib Mineral Petrol* 160:909–930
- Sun S-S, McDonough WF (1989) Chemical and isotopic systematics of oceanic basalts: applications for mantle composition and processes. In: Saunders AD, Norry MJ (eds) *Magmatism in the ocean basins*. Geol Soc, London, Spec Publ 42: 313–345
- Tindle AG, Breaks FW (2000) Columbite-tantalite mineral chemistry from rare-element granitic pegmatites: Separation Lake area, N.W. Ontario, Canada. *Mineral Petrol* 70:165–198
- Uher P, Ondrejka M, Konečný P (2009) Magmatic and post-magmatic Y-REE-Th phosphate, silicate and Nb-Ta-Y-REE oxide minerals in A-type metagranite: an example from the Turčok massif, the Western Carpathians, Slovakia. *Mineral Mag* 73:1009–1025
- Vazquez JA, Velasco NO, Schmitt AK, Black HA, Stelten ME (2014) <sup>238</sup>U-<sup>230</sup>Th dating of chevkinite in high-silica rhyolites from La Primavera and Yellowstone calderas. *Chem Geol* 390:109–118
- Vlach SRF, Gualda GAR (2007) Allanite and chevkinite in A-type granites and syenites of the Graciosa Province, southern Brazil. *Lithos* 97:98–121
- Wise MA, Brown CD (2011) Chemical composition of coexisting columbite-group minerals and cassiterite from the Black Mountain pegmatite, Maine. *Eur J Mineral* 23:817–828
- Wise MA, Černý P, Falster AU (1998) Scandium substitution in columbite-group minerals and ixiolite. *Can Mineral* 36:673–680
- Zhao D, Essene EJ, Zhang Y (1999) An oxygen barometer for rutile-ilmenite assemblages: oxidation state of metasomatic agents in the mantle. *Earth Planet Sci Lett* 166:127–137